Title

Universal relations for compact stars with heavy baryons

Journal

Physical Review C, 108(2)

ISSN

2469-9985

Authors

Li, Jia Jie

Sedrakian, Armen

Weber, Fridolin

Publication Date

2023-08-01

DOI

10.1103/physrevc.108.025810

Universal relations for compact stars with heavy baryons

Jia Jie Li [*]
School of Physical Science and Technology, Southwest University, Chongqing 400715, China

Armen Sedrakian [†]
Frankfurt Institute for Advanced Studies, D-60438 Frankfurt am Main, Germany
and Institute of Theoretical Physics, University of Wroclaw, 50-204 Wroclaw, Poland

Fridolin Weber [‡]
Department of Physics, San Diego State University, 5500 Campanile Drive, San Diego, California 92182, USA
and Center for Astrophysics and Space Sciences, University of California at San Diego, La Jolla, California 92093, USA

(Received 16 May 2023; accepted 2 August 2023; published 18 August 2023)

A set of hadronic equations of state derived from covariant density functional theory and constrained by terrestrial experiments, and astrophysical observations, in particular by the NICER experiment inferences is used to explore the universal relations among the global properties of compact stars containing heavy baryons at high densities. We confirm the validity of universal I-Love-Q relations connecting the moment of inertia (I), the tidal deformability (Λ), and the spin-induced quadrupole moment (Q) for isolated nonrotating stars. We further confirm the validity of the I-C-Q relations connecting the moment of inertia, compactness (C), and quadrupole moment for uniformly and slowly rotating stars, and extend the validity of these relations to maximally rotating sequences. We then investigate the relations between integral parameters of maximally rotating and static compact stars. The universalities are shown to persist for equations of state and compositions containing hyperons and Δ degrees of freedom. When heavy baryons are included, however, the radial profiles of integrands in expressions of global properties exhibit "bumps", which are not present in the case of nucleonic stars in which case the profiles are smooth. We determine the coefficients entering the universal relations in the case of hyperonic and Δ-resonance containing stars.

DOI: 10.1103/PhysRevC.108.025810

I. INTRODUCTION

Compact stars (CSs) as the densest objects in the observable universe form natural astrophysical laboratories for understanding the physics of matter at supranuclear densities [1–13]. Astronomical observations of CSs impose constraints on the behavior of the equation of state (EoS) of dense matter, which is an important input for determining the macroscopic properties of CSs, such as the mass, radius, moment of inertia, etc. The groundbreaking detection of the first gravitational wave (GW) signals from a binary neutron star merger event GW170817 [14,15] has opened a new avenue for studying the internal structure of CSs and the properties of dense stellar matter [16–22]. The x-ray pulse profile modeling of pulsars [23] combined with inferences from the NICER experiment [24–27] led to measurements of CSs' masses and radii. The mass-radius ranges derived for the two-solar mass PSR J0740+6620 are of great value for inferring the properties of dense matter at sufficiently high densities [28–34].

The integral parameters of CSs such as the mass, radius, moment of inertia, quadrupole moment, etc., are controlled by the microscopic EoS of dense matter. Nevertheless, various approximately universal relations connecting different CS integral parameters have been established and intensively studied in recent years [35–76]. Because these relations are insensitive to the input EoS and are held to a high accuracy (the typical deviations are at the level of several per cent), they are called *universal*. The I-Love-Q relations, which connect the moment of inertia I, tidal deformability Λ, and the spin-induced quadrupole moment Q of CSs in slow rotation approximation were first discovered in Refs. [35,36]. These sorts of relations among various integral parameters of CSs have been studied under various conditions such as rapid rotations [43,44,46,47,65,68,70], differential rotations [61,72,76,77], finite temperatures [44,54,56,58,59,64,75], strong magnetic fields [40,78], and within alternative theories of gravity [48,50,71] (for a review, see Ref. [79]). The recent work includes the study of universal relations between the members of the I-Love-Q triple and compactness C (which refers to the equatorial compactness of the star) for slowly rotating CSs [38,39,80–82], and their extension to rapidly rotating stars [43,47]. A different class of universalities can be established between the parameters of static and rotating CSs.

[*]jiajieli@swu.edu.cn
[†]sedrakian@fias.uni-frankfurt.de
[‡]fweber@sdsu.edu

For example, the redshift and maximum mass [59,70,81]. Binary neutron stars merger simulations have also revealed some relations between the properties of the dynamical ejecta and the binary parameters, such as the mass ratio and tidal deformability [67].

The purpose of this work is to test various universal relations for static and rotating CSs using EoSs which account for the presence of heavy baryonic degrees of freedom in ultradense matter. To date, only a handful of studies have tested universal relations using such EoS. This was done for hyperonic matter in Refs. [54–56,58,68,79] and in the case of hyperonic Δ-admixed matter in Ref. [64]. For our purposes, we utilize the EoSs which were previously derived within covariant density functional (CDF) theory including hyperonic and Δ-admixed matter at high densities [22,83–87]. Our EoSs are tuned to satisfy the astrophysical constraints, specifically the mass-radius ranges from NICER inferences [24–27], tidal deformability constraints from the GW event GW170817 [14,15], and the symmetry energy constraints from neutron skin thickness experiment PREX-II [88–91]. The onset of heavy baryons significantly increases the complexity of the EoS, as can be seen by examining the variability of the speed of sound c_s across the star and comparing it with the smooth behavior observed for purely nucleonic EoS models [92,93]. It appears to be an important task to test available universal relations in the case of matter with many particle thresholds and a complex speed of sound behavior, given their significant practical utility and importance. Testing and validating the universal relations for EoS with heavy baryons expands the class of models of the EoS of matter that can be used in astrophysical scenarios which employ universal relations as an integral part of inference of properties of CSs. Such tests are also imperative in view of robust physical arguments in favor of the onset of heavy baryons in dense matter in CSs, as extensively discussed in the literature (for recent arguments see Refs. [11–13] and references therein). Furthermore, the softening associated with heavy baryons is strongly constrained by the observations of two-solar-mass pulsars (addressed in the context of the hyperon puzzle) which allows us to have tight control over the uncertainties in the medium properties of hyperons in nuclear matter. Note that limiting the set of EoSs to those which satisfy the two-solar-mass constraint increases the accuracy to which the universal relations hold [47].

The paper is organized as follows. In Sec. II we introduce the EoS model collection that we employed in our analyses. In Secs. III and IV, we present the universal relations for isolated stars and the universal relation between the parameters of static and rapidly rotating stars, respectively. Finally, a summary of our results is provided in Sec. V. Unless otherwise noted, we use geometric units (where $G = c = 1$) throughout this paper.

II. EOS FOR HADRONIC MATTER

In the present analysis, we adopt the relativistic Hartree (RH) and Hartree-Fock (RHF) [94] descriptions for dense stellar matter, and consider three types of matter compositions:

(1) Purely nucleonic EoS models. We use two representative parametrizations of the nucleonic CDFs, specifically the RHF PKO3 [96] and the RH DDME2 [97] parametrizations. Both of these parametrizations are accurately calibrated by the data on finite nuclei. The predicted maximum mass $M_{\rm max}$ and radius $R_{1.4}$ of canonical-mass $1.4\,M_\odot$ stars are $M_{\rm max} = 2.49\,M_\odot$, $R_{1.4} = 13.96$ km for PKO3 [94] and $M_{\rm max} = 2.48\,M_\odot$, $R_{1.4} = 13.22$ km for DDME2 [94]. This class of models is labeled as "N". These nucleonic models produce massive neutron stars, which guarantees that in the case of moderate softening due to the onset of hyperons, the maximum masses of hyperonic stars reach a value of $2\,M_\odot$ as required by the observations.

(2) Hyperonic EoS models. We extend the two nucleonic models mentioned above to the hyperonic sector by adjusting the meson-hyperon coupling constants to reproduce the empirical potentials of hyperons in nuclear matter. As a result, we are able to generate hyperonic stars with masses around $2\,M_\odot$. In particular, for the RH model, the vector meson-hyperon couplings are fixed by the SU(6) spin-flavor symmetric model, with the scalar σ-meson-hyperon couplings defined by their ratios $R_{\sigma\Lambda} = 0.6105$, $R_{\sigma\Sigma} = 0.4426$, and $R_{\sigma\Xi} = 0.3024$ to the corresponding nucleonic couplings (see Ref. [13] for a discussion). For the RHF model, the vector meson-hyperon couplings are determined by the SU(3) flavor symmetric model, to obtain more repulsion in the hyperonic sector to counterbalance the softening due to the Fock terms [94]. These two hyperonic EoS models are labeled as "NY". Further EoS models that will be used below are based on the RH model but have broken SU(6) quark symmetry in the vector meson sector, as explained in Ref. [98]. This allows us to have hyperonic models with maximum masses in the range $2.1 \lesssim M_{\rm max} \lesssim 2.4\,M_\odot$. This class of models is labeled as "NY(a)–(e)".

(3) Hypernuclear models with an Δ admixture. These models are the same as the two hyperonic models "NY" above but include in addition the quartet of spin-3/2 Δ resonances. As no consensus has been reached yet on the magnitude of the Δ potential in nuclear matter, we take three suggested values for the depth of the Δ potential, $V_\Delta(\rho_{\rm sat}) = (1 \pm 1/3)V_N(\rho_{\rm sat})$, where $V_N(\rho_{\rm sat})$ is the nucleonic potential at saturation density. This class of models is labeled as "$NY\Delta$(a)–(c)". The main difference caused by the inclusion of Δ's is the reduction of the star's radius by up to 1–2 km at central stellar densities slightly above the nuclear saturation density [83].

Figure 1(a) shows the EoSs included in our collection. The squared speed of sound, c_s^2, obtained with these models is shown in Fig. 1(b). It is seen that EoSs containing only nucleonic degrees of freedom have a c_s^2 that monotonically increase with increasing baryon number density ρ (or energy density ε). The appearances of hyperons and Δ particles change the shape of the curves to non-monotonic forms which reflects the nucleation of new degrees of freedom. The onset of heavy baryons reduces the speed of sound abruptly. Interestingly, in the case of an early appearance of Δ particles (at $\rho \sim 1.5\rho_{\rm sat}$), the speed of sound drops to zero indicating a possible region of instability associated with a liquid-gas type phase transition [99].

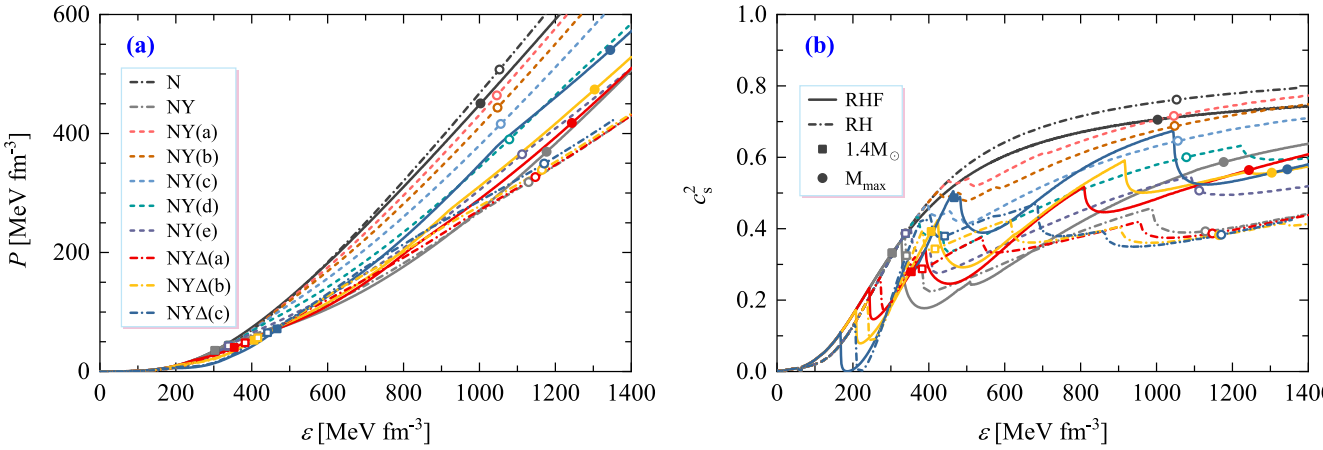

FIG. 1. EoSs for stellar matter featuring different compositions, i.e., nucleonic (N), hyperonic (NY), and hyperon-Δ admixed ($NY\Delta$) one (a), and the associated speed of sound squared c_s^2 (b). The results are obtained using both the RHF and RH approaches. The positions for canonical-mass and maximum-mass configurations are marked by squares and circles.

Figure 2 shows the mass-radius relations of static and maximally rotating, hereafter referred also as *Keplerian*, CSs. Additionally, the results include (a) the 68.3% credible interval for the mass and radius estimates of PSR J0030+0451 [24,25] and PSR J0740+6620 [26,27] as well as (b) the range of masses extracted for the secondary object in the GW190814 event [95]. It is seen that the masses and radii of static configurations based on our EoS collection cover ranges of $2.0 \lesssim M_{\rm max} \lesssim 2.5\,M_\odot$ and $12 \lesssim R_{1.4} \lesssim 14$ km, i.e., our EoSs predict models that are consistent with the current astrophysical constraints.

Maximally rotating stars have masses approximately 20% larger than their static counterparts because the centrifugal force provides additional support against the gravitational pull toward the center of the star. Their equatorial radii are about 40% larger than the radii of static stars. It is seen that the maximum values for mass and radius of Keplerian configurations in our model collection cover the ranges $2.5 \lesssim M_{\rm max} \lesssim 3.0\,M_\odot$ and $17 \lesssim R_{1.4} \lesssim 20$ km.

III. UNIVERSAL RELATIONS FOR ISOLATED CSS

In this section, we investigate whether the universal relations among integral quantities such as the mass, radius, moment of inertia, and quadrupole moment maintain their validity for static and rotating CSs with heavy baryons in their centers, in particular, those possessing hyperon-Δ admixed cores.

A. Static and slowly rotating CSs

The tidal deformability of static CS scales as $\Lambda \propto k_2 C^{-5}$, according to Eq. (A4). The analytical form of the Love number k_2 is complicated, but the numerical evaluations of k_2 shown in Fig. 3 for $C \gtrsim 0.1$ (which is equivalent to $M \gtrsim 1.0\,M_\odot$) show that k_2 scales approximately as C^{-1} and saturates for $C \approx 0.1$ [22,100]. Therefore, the scaling becomes $\Lambda \propto C^{-6}$ or $C \propto \ln \Lambda$ for masses in the interval $1.0 \lesssim M \lesssim 2.0\,M_\odot$, which is the mass range of phenomenological interest. The latter scaling behavior can be clearly observed in

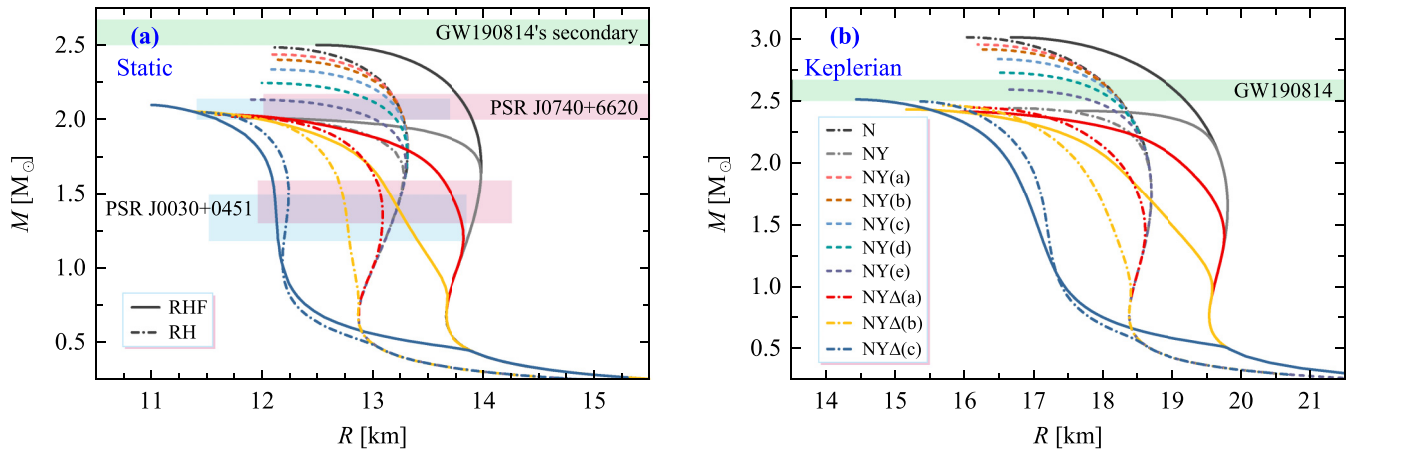

FIG. 2. Mass-radius relations of CSs in the static and maximally rotating (Keplerian) limits for various EoS models. The masses and radii for PSR J0030+0451 [24,25] and PSR J0740+6620 [26,27] (68.3% credible interval) are inferred from NICER data, and the mass range extracted for the secondary of the GW190814 event [95] is shown as well.

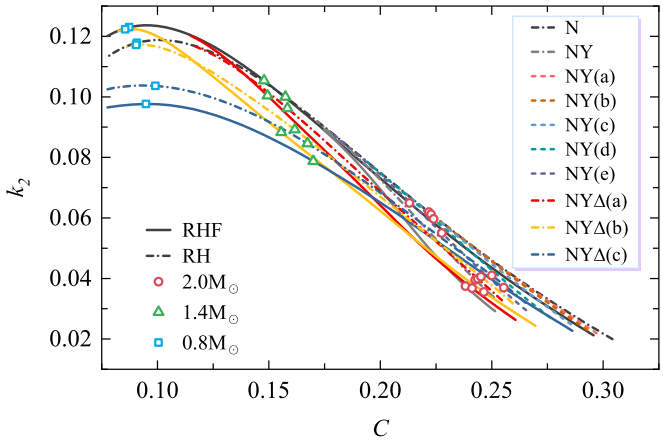

FIG. 3. The dimensionless tidal Love number k_2 as a function of compactness C for hadronic EoS. The squares, triangles, and circles indicate configurations with $M = 0.8$, 1.4, and $2.0\,M_\odot$, respectively.

Fig. 4, where the values of Λ are shown on a logarithmic scale.

Building on the aforementioned scaling, one could hypothesize a scaling formula like

$$C = \sum_{n=0}^{m} a_n (\ln \Lambda)^n, \tag{1}$$

which was explored in Ref. [38] for $m = 2$. The author of that paper used three EoS models (including a hybrid star model) with a mass interval $1.2 \leqslant M \leqslant 2.0\,M_\odot$, and found the relation to be accurate up to 2%. Later, this hypothesis was confirmed by Yagi *et al.* in Ref. [79] through the examination of a comprehensive collection of 25 hadronic EoS models, which included five hyperonic models, and found that the maximum deviation is somewhat larger ∼6.5%. Recently, the same relation was tested for hot EoS appropriate for protoneutron stars [64] and was found to hold with the same level of accuracy for stars with fixed entropy per baryon and lepton fraction, i.e., fixed thermodynamic conditions. Below we will utilize Eq. (1) truncated at $m = 4$, which is a polynomial degree employed in other universal relations examined in this work as well.

Figure 4 shows C-$\ln\Lambda$ relation for our collection of EoS in the case of static CSs according to Eq. (1) with $m = 4$. The bottom panel presents the fractional difference between the data and the fit. It is seen that the deviation is at the level of a few percent. The best-fit coefficients are summarized in Table I for $m = 2$ and $m = 4$. The coefficients for $m = 2$ obtained for our collection of EoSs are in agreement with those found in Ref. [79].

We now turn to the universal relations associated with the I-Love-Q relation for our collection of EoSs. Before showing

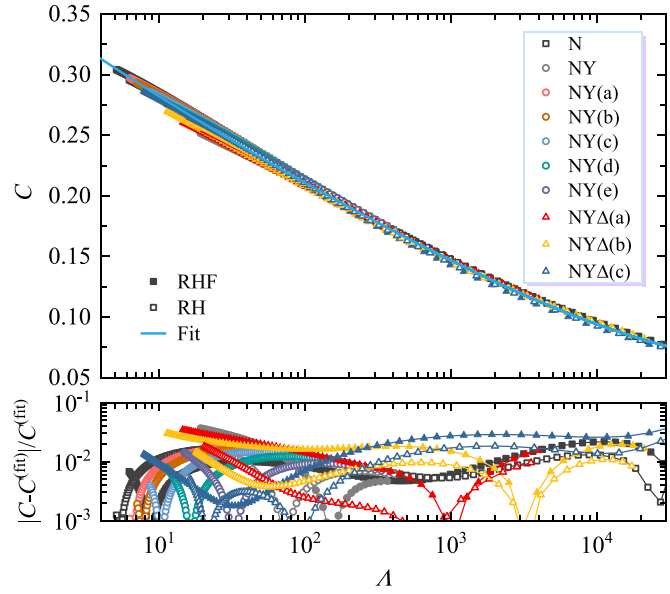

FIG. 4. The C-Love relations for static hadronic CSs. (Top) Universal relations for various EoS models together with their fitting curves. (Bottom) Fractional errors between the fitting curve and numerical results.

the results, let us note that for a uniform Newtonian star one has [36]

$$\Lambda = \tfrac{1}{2}C^{-5}, \quad \bar{I} = \tfrac{2}{5}C^{-2}, \quad \bar{Q} = \tfrac{25}{8}C^{-1}, \tag{2}$$

which translate into

$$\bar{I} \propto \Lambda^{2/5}, \quad \bar{Q} \propto \Lambda^{1/5}, \quad \bar{Q} \propto \bar{I}^{1/2}. \tag{3}$$

Equations (2) and (3) provide useful guidance for choosing the functional forms of universal relations for relativistic CSs.

The universal relations of Λ, $\bar{I}$, and $\bar{Q}$ can be explored using the scheme suggested in Refs. [35,36],

$$\ln y = \sum_{n=0}^{4} a_n (\ln x)^n, \tag{4}$$

where the pairs (x, y) represent $(\Lambda, \bar{I})$, $(\Lambda, \bar{Q})$, and $(\bar{Q}, \bar{I})$. Figure 5 shows these three combinations for CSs containing heavy baryons together with the fits according to Eq. (4). The bottom panels of this figure show the fractional differences between the data and the fits. The moment of inertia and the quadrupole moment were computed assuming the slow rotation approximation up to second order. It is seen that the absolute fractional differences of these relations are $\lesssim 1\%$ for all three relations. The best-fit coefficients with Eq. (4) are

TABLE I. Estimated coefficients for the universal C-Love relation. The corresponding reduced χ-squared (χ^2_{red}) values are shown in the last column.

y	x	a_0	a_1	a_2	a_3	a_4	χ^2_{red}
C	Λ	3.63278×10^{-1}	-3.84806×10^{-2}	1.77351×10^{-3}	-1.78329×10^{-4}	1.03106×10^{-5}	7.82102×10^{-6}
		3.63958×10^{-1}	-3.74047×10^{-2}	8.87636×10^{-4}			8.22215×10^{-6}

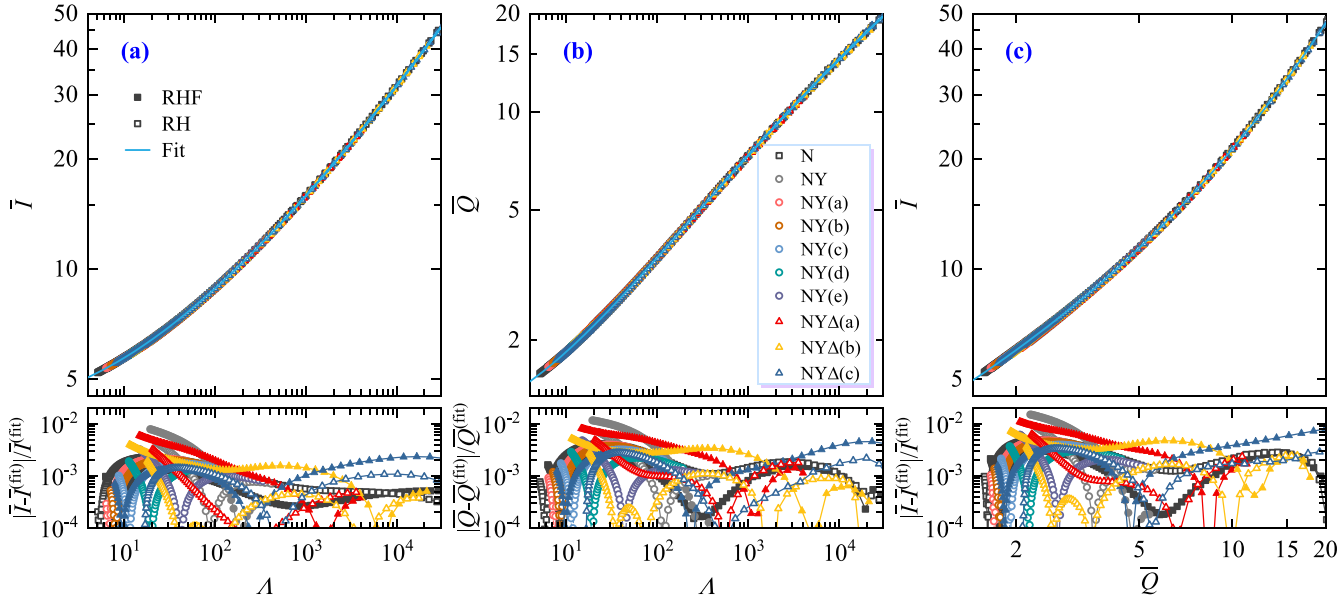

FIG. 5. The $\bar{I}$-Love-$\bar{Q}$ relations for hadronic CSs within the slow-rotation approximation. (Top) Universal relations for various EoS models together with their fitting curves. (Bottom) Fractional errors between the fitting curves and numerical results.

summarized in Table II, which are consistent with those found in Ref. [79].

Because of the universality of the C-$\ln\Lambda$ relation and the universality among $\bar{I}$-Λ-$\bar{Q}$, it can be postulated that the relations $\bar{I}$-C and $\bar{Q}$-C also exhibit universality. The $\bar{I}$-C and $\bar{Q}$-C universal relations were investigated in Refs. [36,47,64,68,82] by exploring their functional forms with the inverse compactness C^{-1} serving as the independent variable. Below, we will concentrate on this dependence, i.e.,

$$\bar{I} = \sum_{n=0}^{m} a_n (C^{-1})^n, \quad \bar{Q} = \sum_{n=0}^{m} a_n (C^{-1})^n \tag{5}$$

with $m = 4$. For a large set of EoS the relation for $\bar{I}$ was found to be universal, with relative deviations being on the order of 10%. Reference [64] considered also the universality of the second relation in Eq. (5) for $m = 3$. These universal relations (5) where extended to a set of finite-temperature hadronic EoS models (including two hyperonic and one hyperon-Δ admixed EoS models based on the DDME2 parametrization) in the case of fixed entropy per baryon and fixed lepton fraction. The universality holds with the same level of accuracy for both cold and hot stars, provided the thermodynamic parameters within the EoS are the same.

Figure 6 shows $\bar{I}$ and $\bar{Q}$ as a function of C, and the $\bar{I}$-$\bar{Q}$ relation for sequences computed using the slow-rotation approximation ($\chi \ll 1$), together with rapidly rotating sequences with fixed spin parameters χ ($\chi \equiv J/M^2$ with J being the angular momentum of the star), and the maximally rotating sequence. The subsequent subsections will discuss the latter two categories of sequences. In panels (a) and (b), we present for each $\bar{I}$-C or $\bar{Q}$-C relation two fitting curves, one using Eq. (5) and one dropping the zeroth order term. In panel (c), each relation is shown by a single curve given by Eq. (4). Table III summarizes the coefficients for these universal relations, along with the corresponding reduced χ-squared χ^2_{red} values (which are obtained by dividing the residual sum of squares by the degrees of freedom). The fractional differences are shown in the lower panels of Fig. 6 whereby those for panels (a) and (b) are evaluated with respect to fits that use Eq. (5). As can be seen in Fig. 6, the maximum fractional differences are close to 7–8% for the $\bar{I}$-C and $\bar{Q}$-C relations, which can be compared to the $\bar{I}$-Λ and $\bar{Q}$-Λ universal relations where the deviations were mostly below 1%.

B. Rapidly rotating CSs

We next test the validity of the universal relations among $\bar{I}$, $\bar{Q}$, and C for rapidly rotating CSs. Note that compactness

TABLE II. Estimated coefficients for the universal $\bar{I}$-Love, $\bar{Q}$-Love, and $\bar{I}$-$\bar{Q}$ relations obtained in the slow-rotation approximation. The corresponding reduced χ-squared (χ^2_{red}) values are shown in the last column.

y	x	a_0	a_1	a_2	a_3	a_4	χ^2_{red}
$\bar{I}$	Λ	1.49834×10^{0}	5.83188×10^{-2}	2.26613×10^{-2}	-7.15384×10^{-4}	8.60779×10^{-6}	2.91090×10^{-6}
$\bar{Q}$	Λ	1.95655×10^{-1}	9.02591×10^{-2}	4.87888×10^{-2}	-4.39624×10^{-3}	1.30998×10^{-4}	8.02989×10^{-6}
$\bar{I}$	$\bar{Q}$	1.39803×10^{0}	5.35419×10^{-1}	3.82137×10^{-2}	1.81689×10^{-2}	1.92556×10^{-4}	1.30642×10^{-5}

TABLE III. Estimated coefficients for the universal $\bar{I}$-C, $\bar{Q}$-C, and $\bar{I}$-$\bar{Q}$ relations. The corresponding reduced χ-squared ($\chi^2_{\rm red}$) values are shown in the last column.

y	x	χ	a_0	a_1	a_2	a_3	a_4	$\chi^2_{\rm red}$
$\bar{I}$	C	$\ll 1$	2.78328×10^{0}	-9.28412×10^{-1}	6.01079×10^{-1}	-3.26388×10^{-2}	8.30545×10^{-4}	6.51045×10^{-2}
				7.52174×10^{-1}	2.49719×10^{-1}	-2.52963×10^{-3}	-7.00854×10^{-5}	6.68638×10^{-2}
		0.2	2.40576×10^{0}	-6.98316×10^{-1}	5.53941×10^{-1}	-2.92220×10^{-2}	7.29404×10^{-4}	1.01976×10^{-1}
				7.15632×10^{-1}	2.66210×10^{-1}	-5.15035×10^{-3}	2.40009×10^{-5}	1.03497×10^{-1}
		0.4	2.28723×10^{0}	-6.25782×10^{-1}	5.35113×10^{-1}	-2.81811×10^{-2}	6.89230×10^{-4}	1.22620×10^{-1}
				7.09692×10^{-1}	2.65274×10^{-1}	-5.77664×10^{-3}	3.78995×10^{-5}	1.23993×10^{-1}
		0.6	2.03438×10^{0}	-4.04730×10^{-1}	4.57441×10^{-1}	-2.16860×10^{-2}	4.36667×10^{-4}	2.75660×10^{-1}
				7.52295×10^{-1}	2.30435×10^{-1}	-3.43435×10^{-3}	-7.60088×10^{-5}	2.76760×10^{-1}
		Kep.	1.59880×10^{0}	-6.12213×10^{-2}	3.26296×10^{-1}	-1.47631×10^{-2}	2.97495×10^{-4}	1.43312×10^{-1}
				7.53968×10^{-1}	1.83664×10^{-1}	-4.57602×10^{-3}	4.39646×10^{-5}	1.44235×10^{-1}
$\bar{Q}$	C	$\ll 1$	1.09156×10^{0}	-1.19359×10^{0}	5.12662×10^{-1}	-3.61313×10^{-2}	9.18768×10^{-4}	1.01870×10^{-2}
				-5.34487×10^{-1}	3.74863×10^{-1}	-2.43229×10^{-2}	5.65554×10^{-4}	1.04575×10^{-2}
		0.2	0.83661×10^{0}	-9.49862×10^{-1}	4.42625×10^{-1}	-3.01219×10^{-2}	7.41153×10^{-4}	1.43124×10^{-2}
				-4.58158×10^{-1}	3.42566×10^{-1}	-2.17509×10^{-2}	4.95847×10^{-4}	1.44944×10^{-2}
		0.4	1.17854×10^{0}	-9.62231×10^{-1}	3.98228×10^{-1}	-2.63341×10^{-2}	6.39743×10^{-4}	1.43084×10^{-2}
				-2.74102×10^{-1}	2.59188×10^{-1}	-1.47897×10^{-2}	3.04132×10^{-4}	1.46898×10^{-2}
		0.6	1.38135×10^{0}	-8.18944×10^{-1}	3.03745×10^{-1}	-1.83139×10^{-2}	4.03007×10^{-4}	2.60640×10^{-2}
				-3.33255×10^{-2}	1.49608×10^{-1}	-5.92101×10^{-3}	5.49006×10^{-5}	2.66705×10^{-2}
		Kep.	0.93212×10^{0}	-3.89707×10^{-1}	1.70288×10^{-1}	-8.73106×10^{-3}	1.71199×10^{-4}	1.51724×10^{-3}
				8.55566×10^{-2}	8.71318×10^{-2}	-2.79190×10^{-3}	2.33887×10^{-5}	1.88169×10^{-3}
$\bar{I}$	$\bar{Q}$	$\ll 1$	1.39803×10^{0}	5.35419×10^{-1}	3.82137×10^{-2}	1.81689×10^{-2}	1.92556×10^{-4}	1.30642×10^{-5}
		0.2	1.38034×10^{0}	5.85404×10^{-1}	1.91033×10^{-2}	2.26290×10^{-2}	-3.53397×10^{-4}	1.42634×10^{-5}
		0.4	1.35669×10^{0}	7.04071×10^{-1}	-2.36864×10^{-2}	3.28473×10^{-2}	-1.86181×10^{-3}	1.19826×10^{-5}
		0.6	1.31300×10^{0}	9.21151×10^{-1}	-1.28186×10^{-1}	6.18742×10^{-2}	-5.65783×10^{-3}	1.50910×10^{-5}
		Kep.	1.29830×10^{0}	1.02524×10^{0}	-1.75735×10^{-1}	7.80475×10^{-2}	-8.85528×10^{-3}	1.78771×10^{-4}

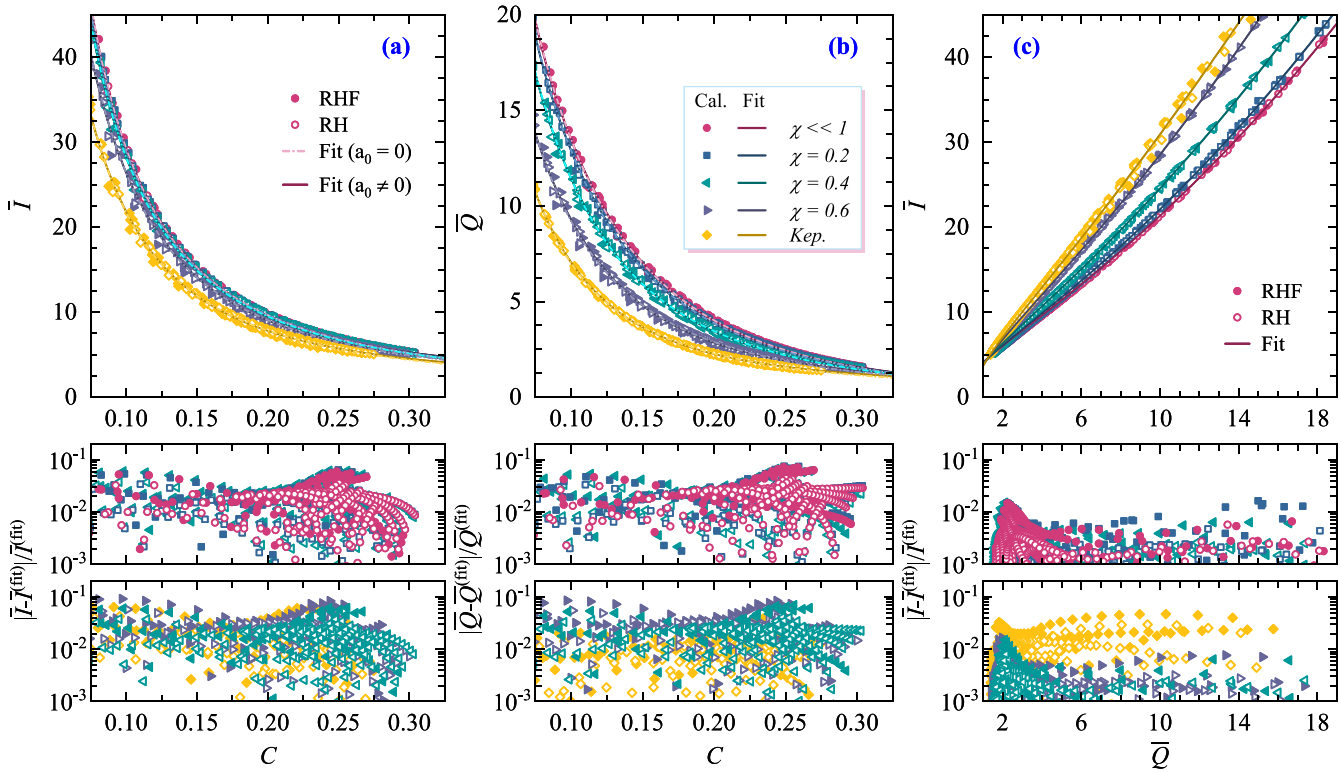

FIG. 6. The $\bar{I}$-C-$\bar{Q}$ relations for rotating hadronic CSs along sequences with constant spin parameter χ. (Top) Universal relations for various EoS models together with the fitting curves. (Bottom) Fractional errors between the fitting curves and numerical results.

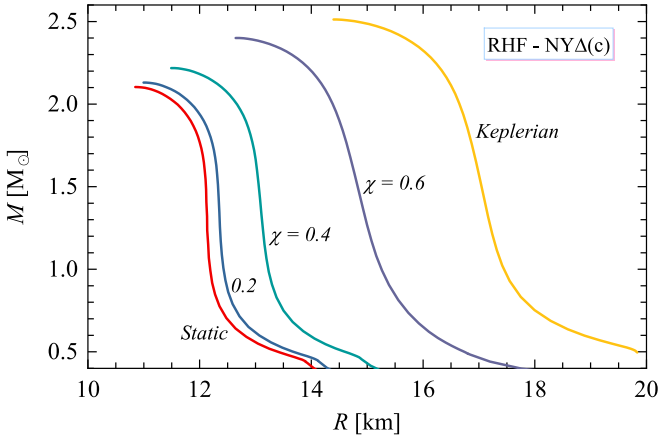

FIG. 7. The mass-radius relations of CSs for different rotation rates, namely static, rapidly rotating with constant spin parameters of $\chi = 0.2$, 0.4, and 0.6, as well as the maximum rotation rate (Keplerian limit), using the RHF EoS of $NY\Delta$ (c).

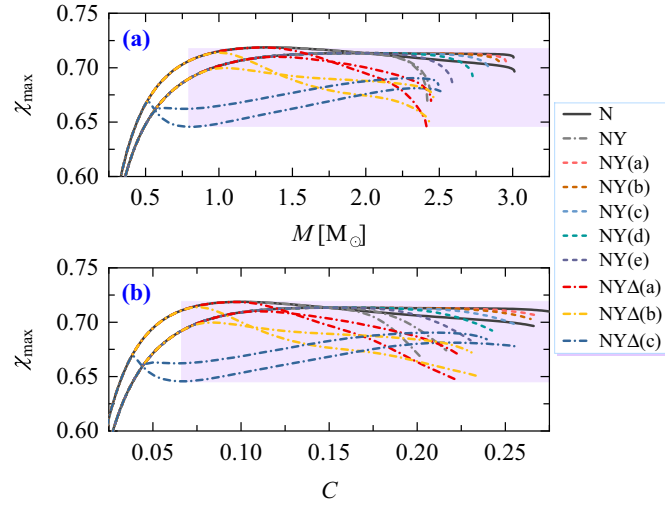

FIG. 8. The maximum spin parameter $\chi_{\max}$ as function of gravitational mass M (a) and compactness C (b) for hadronic CSs.

in this case is defined using the equatorial radius. In this case, the universal relations are commonly investigated for a sequence of stars with constant values of certain parameters characterizing the magnitude of rotation.

The universality of the $\bar{Q}$-$\bar{I}$ relation holds for stellar sequences with fixed dimensionless spin parameter $\chi = J/M^2$ [41] and $\tilde{f} = Rf$, where f is the spin frequency [43], but not for stars with constant spin frequency f [37]. The $\bar{Q}$-$\bar{I}$ relation was found for fixed χ and $\tilde{f}$ to be nearly independent of the EoS with a relative error $\sim$1%, i.e., with an error comparable to the slow-rotation case. In addition, Ref. [47] found universality of $\bar{I}$-C relation for rotating nucleonic CSs for three values of the spin parameter. The universal relations for hot and maximally fast rotating CSs were established in Ref. [68].

Below we will show universal relations for sequences with constant spin parameters of $\chi = 0.0$, 0.2, 0.4, and 0.6, as well as the Keplerian limit. The mass-radius relations of these sequences are shown in Fig. 7 for our RHF EoS model with $NY\Delta$ composition. It is observed that these relations are self-similar for different values of the spin parameter χ.

Our results for $\bar{I}$-C-$\bar{Q}$ relations are presented in Fig. 6 for the χ values quoted just above. As in the nonrotating case, the $\bar{I}$-C and $\bar{Q}$-C relations are fitted with two different functions: one is given by the full Eq. (5) and the other with a vanishing zero-order term. The fractional differences are estimated for the full expression. For the $\bar{Q}$-$\bar{I}$ relation the fitting curves are given by Eq. (4).

It is seen in Fig. 6 that the fractional differences are comparable in magnitude for all values of the spin parameter and for the static case. The $\bar{I}$-C and $\bar{Q}$-$\bar{I}$ relations for each sequence are self-similar and tend to a single value in the extreme "black hole" limit where $\bar{I} \to 4$ and $\bar{Q} \to 1$ when $C \to 0.5$. Again, as in the static case, the $\bar{Q}$-$\bar{I}$ relation holds to higher accuracy for all sequences. The maximum absolute fractional difference is between about 1–2%, which is comparable to that for static stars.

CSs reach the limit of stability for uniform rotation at the Keplerian limit, where the centrifugal and gravitational forces at the equator of the star are balanced. Beyond this frequency, mass is shed from the equator. A convenient parameter for locating the Keplerian limit is the spin parameter χ [98,101]. In Fig. 8 we plot the maximum spin parameter $\chi_{\max}$ versus gravitational mass and compactness for CSs constructed from our collection of EoS. It is seen that $\chi_{\max}$ increases with mass in the domain $M < 1.0\,M_\odot$ and then (a) stays constant for purely nucleonic EoS models; (b) it is reduced for models which contain hyperons; (c) the reduction is more pronounced for models that have in addition to hyperons a Δ-resonance admixture in their cores. Thus, the $\chi_{\max}$ as a function of mass M or compactness C can no longer be monotonic; this is more prominent for the $NY\Delta$ models. The value of $\chi_{\max}(M)$ or $\chi_{\max}(C)$ is noteworthy in that all models fall within a narrow range of 0.64–0.72, as indicated by the shaded region in Fig. 8. The values of $\chi_{\max}$ derived for our EoS collection are consistent with those found in Refs. [98,101–103].

Figure 6 also shows $\bar{I}$-C-$\bar{Q}$ relations for Keplerian sequences. In this case, the fractional difference for the $\bar{I}$-$\bar{Q}$ relation increases to 5%, because $\chi_{\max} = 0.68 \pm 0.04$ for different EoS, i.e., it is not constant anymore but lies in the indicated range. The fractional differences for the $\bar{I}$-C and $\bar{Q}$-C relations remain comparable to those for static and constant spin sequences. The fit coefficients in the universal relations for our sequences with constant χ, including the Keplerain sequences, are summarized in Table III. Also provided in this table are the corresponding reduced χ-squared (χ^2_{red}) values.

The universalities shown in Fig. 6 allow (in principle) the determination of the radius of a pulsar, if the mass and one of the quantities $\bar{I}$ and $\bar{Q}$ are sufficiently well measured. The mass in binaries containing a neutron star (pulsar) can be measured by the relativistic Shapiro delay. Then, according to the definitions of $\bar{I}$ or $\bar{Q}$, the radius of the pulsar can be derived. We note, however, that the $\bar{I}$ and $\bar{Q}$ are largely degenerate for pulsars with a small value of spin or a large value of compactness. This makes it very challenging to measure the

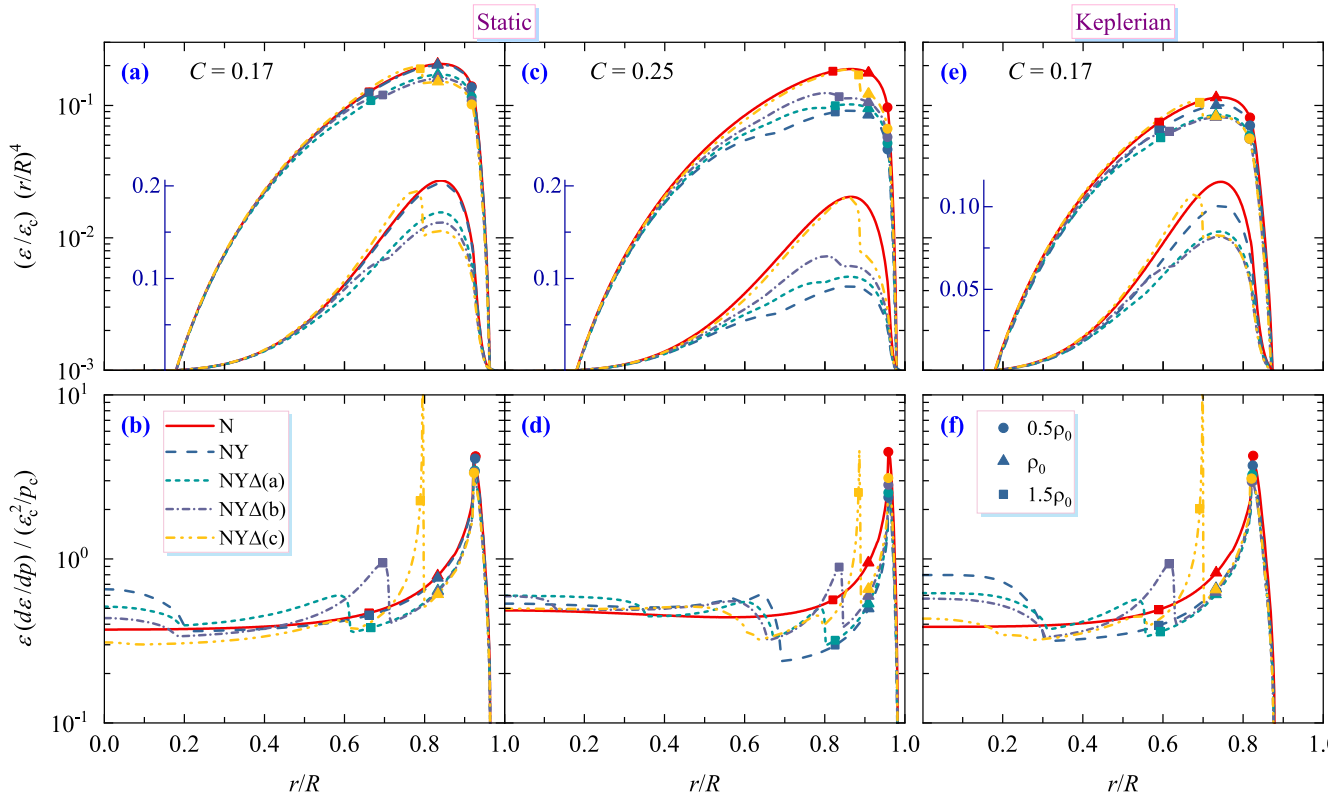

FIG. 9. The normalized radial profiles $[(\varepsilon/\varepsilon_c)/(r/R)^4]$ and $[\varepsilon(d\varepsilon/dp)/(\varepsilon_c^2/p_c)]$ as a function of r/R for static (left panels) CSs with compactness $C = 0.17$, 0.25, and Keplerian rotating (right panels) CSs with $C = 0.17$. The results are calculated with the RHF models for various particle compositions. The positions of the crust-core transition ($\sim 0.5\,\rho_0$) and 1.0, $1.5\,\rho_0$ are marked. In the top panels, the data are shown on a linear scale, too.

radius of a pulsar from the moment of inertia I, or quadrupole moment Q independently.

C. Radial profiles of CSs

Several hypotheses for the origin of universalities were put forward early on in Refs. [35,36], but their physics remains a matter of debate. It has been pointed out that the contribution of the outer stellar layer, where the physics is mostly settled, may render the integral parameters insensitive to the details of the CS's physics at higher densities. It has also been pointed out that universalities could be reminiscent of the no-hair theorems for black holes. For models with compactness approaching the black-hole limit, the details of the internal structure may become unimportant. We will discuss these points below using our collection of EoSs.

To gain insight into the origin of universalities it is useful to investigate the radial dependence of quantities of interest. In Fig. 9, we present the (normalized) radial profiles $[\varepsilon r^4/\varepsilon_c R^4]$ and $[\varepsilon(d\varepsilon/dp)/(\varepsilon_c^2/p_c)]$ for static (left panels) CSs with compactnesses $C = 0.17$, 0.25, as well as Keplerian rotating (right panels) CSs with compactness $C = 0.17$. Here, ε_c and p_c are the central energy density and the corresponding pressure, respectively, and R is the equatorial radius. These results were obtained using RHF EoS with various N, NY, and $NY\Delta$ compositions. The sudden changes in the slope of each the curve are associated with the crust-core transition and the onsets of various species of heavy baryons. For static configurations, the plotted quantity $[\varepsilon r^4]$ appears in the integrands of the moment of inertia and quadrupole moment in the Newtonian limit, whereas the quantity $[\varepsilon(d\varepsilon/dp) = \varepsilon c_s^2]$ appears in the integrand of tidal deformability [36].

The top panels of Fig. 9 show the quantity $[\varepsilon r^4]$, which is relevant for I and Q. It is seen in Fig. 9(a), where $C = 0.17$, that the profiles of this quantity are the same for $r/R < 0.6$ and $r/R > 0.9$. Noticeable differences appear within the range $0.6 \leqslant r/R \leqslant 0.9$ with the maxima of the curves differing by up to 30%. This range corresponds to the low-density regions around the nuclear saturation density, which dominantly contributes to I and Q. For more compact stars with $C = 0.25$, shown in Fig. 9(c), noticeable deviations appear already for $r/R \geqslant 0.5$, with variations of up to 50% at the maxima located at $r/R \approx 0.8$. The profiles of Keplerian models with $C = 0.17$, shown in panel (e), can now be compared to those of the static CSs with the same compactness. This comparison shows the same qualitative behavior but with lower values of the maxima.

The bottom panels of Fig. 9 show the profile of $[\varepsilon(d\varepsilon/dp)]$ relevant for tidal deformability. It is seen that for the case $C = 0.17$, shown in Fig. 9(b), peaks appear close to the crust-core transition and within the range $0.6 \lesssim r/R \lesssim 0.8$ due to the onset of heavy baryons. The radial profiles of more compact stars with $C = 0.25$, shown in Fig. 9(d), have a similar

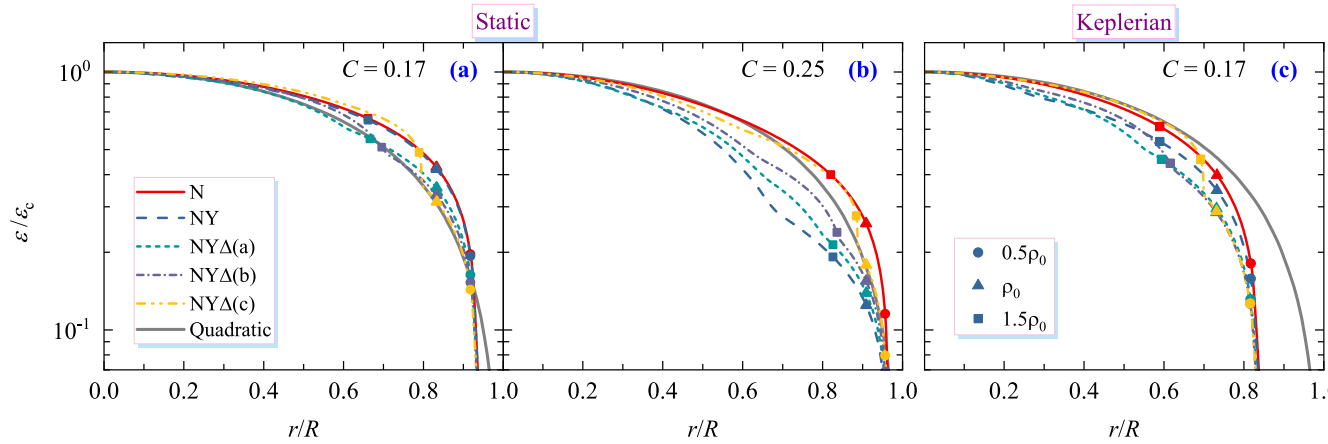

FIG. 10. The normalized radial density profiles $[\varepsilon/\varepsilon_c]$ as a function of r/R for static (left panels) CSs with compactness $C = 0.17$, 0.25, and Keplerian rotating (right panels) stars with $C = 0.17$. The profiles of a quadratic model for $\varepsilon/\varepsilon_c$ (see text) are shown as well.

structure to the previous case, with substantial (quantitatively similar) deviations between different EoSs in the range $0.6 \lesssim r/R \lesssim 0.9$.

Our results above provide no evidence that the $\bar{I}$-C-$\bar{Q}$ universality results from the independence of the profiles of the integrands of these global quantities for our collection of EoSs in the outer core and the crust. In fact, while the EoSs in the low density range $\rho/\rho_0 \leqslant 1.5$ are similar, the profiles of relevant quantities as a function of *normalized* radius, as illustrated in Fig. 9, are closely matched only in the innermost core regions and the outermost crustal regions. Consider now the interval $0.5 \lesssim r/R \lesssim 0.9$, where deviations are observed. We note that the functional behavior (increase or decrease) of $[\varepsilon r^4]$ with r/R is similar to that of the quantity $[\varepsilon(d\varepsilon/dp)]$. This "correlation" is best seen for $C = 0.25$. Therefore, one may conclude that the high level of universality of $\bar{I}$-Λ-$\bar{Q}$ relations is mainly attributed to the "correlation" between the underlying profiles of $\bar{I}(\bar{Q})$-C and $\bar{\Lambda}$-C, which leads to a cancellation when combined.

Among the various suggestions proposed to explain the origin of universality, Ref. [42] put forward the idea that the assumption of self-similarity of isodensity contours in realistic CSs, which can be approximated by elliptical contours, plays a crucial role in the universality of I-Love-Q relations. Furthermore, in Ref. [104] numerical evidence was presented that demonstrated that the universality, which holds in the incompressible limit and implies self-similar isodensity surfaces, is retained for modern realistic EoSs. These EoSs are known to be stiff and, thus, have also self-similar isodensity surfaces. Another hypothesis proposed in Ref. [62] suggests that the universal relations arise from the fact that the energy density of a realistic CS can be approximated as a quadratic function of the normalized radius, given by $\varepsilon(r/R) = \varepsilon_c[1 - (r/R)^2]$, where ε_c is the central stellar energy density.

In Fig. 10, we present the radial profiles of energy density $[\varepsilon/\varepsilon_c]$, together with the ones from the quadratic model. This allows one to account for the difference between the realistic CS profile and that of the quadratic model. It is seen that the density profiles of less compact static stars, $C = 0.17$, can be approximated with an accuracy of up to 30% (except for the crust region) with the quadratic model, whereas for more compact static stars, e.g., for $C = 0.25$, or for rapidly rotating stars, the profiles deviated strongly from a quadratic one.

In closing, it is worth noting that the integrand of the mass M, which is given in terms of $[\varepsilon r^2]$, varies with r/R like the normalized energy density shown in the top panels of Fig. 9. Because mass enters the definitions of the dimensionless quantities $\bar{I}$ and $\bar{Q}$, the similarity in the variations of the integrands of these quantities may partially cancel each other out.

In conclusion, it appears that the universal relations discussed above do not depend on specific details of the EoS but rather result from an overall self-similar behavior of the integrands of global quantities. The radial profiles of integrands of quantities observed in purely nucleonic EoS models do not exhibit self-similarity in the presence of heavy baryons, as revealed by our results. Given that these relations hold for EoSs that include heavy baryons, it is evident that the mere similarity of the radial profiles is not sufficient to guarantee universality.

IV. UNIVERSAL RELATIONS BETWEEN THE KEPLERIAN SEQUENCE AND ITS NONROTATING COUNTERPART

In this section, we turn our attention to a particular class of universal relations, which are related to the integral parameters of static and maximally (Keplerian) rotating stars. Phenomenologically, it is relevant to study stellar sequences with constant baryonic mass $M_{\rm B}$. Evolutionary sequences that lie between the limiting cases of static stars with mass and radius $M_{\rm S}$ and $R_{\rm S}$, and Keplerian stars with mass and equatorial radius $M_{\rm K}$ and $R_{\rm K}$, are often employed to simulate the spin-down or spin-up of stars under external torques. These torques can be generated by electromagnetic and gravitational radiation (resulting in spin-down), or accretion (resulting in spin-up). A typical case is that of a CS that is born in a supernova and spins down primarily due to the emission of magnetic-dipole radiation and a wind of electron-positron pairs, along the evolutionary sequence of constant baryonic mass.

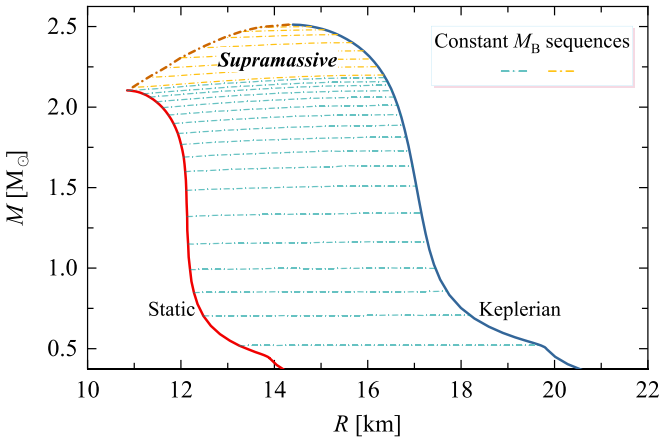

FIG. 11. Schematic plot showing constant baryonic mass sequences calculated with the RHF EoS of $NY\Delta$ (c). The supramassive class of stars is sustained by uniform rotation and lacks a static counterpart.

To illustrate this, Fig. 11 shows sequences of constant baryonic mass (M_B) calculated using the RHF EoS of $NY\Delta$(c). It is seen that these sequences represent almost horizontal lines connecting the Keplerian limiting configuration with the nonrotating one. Note that the true physical stability may not terminate at the Keplerian limit as various instabilities may set in at smaller rotation rates [105,106]. The sequences shown can be classified into two categories—one that does have a nonrotating stable limit and those with larger masses which do not. The first category includes stars with a static configuration mass equal to or less than the maximum mass. The second category comprises stars that do not have a nonrotating member and are known as supramassive CSs. In this category, all the stars are unstable and terminate in a black hole beyond the maximum star limit for any fixed rotation rate.

A. Relating mass, radius, and compactness of static and Keplerian sequences

Figure 12 depicts the mass, radius, and compactness of Keplerian CSs vs the same quantities for their static counterparts for a fixed baryonic mass of the star M_B value for our EoS collection. In practice, we find for any M_S the corresponding value of M_B and then find the Keplerian configuration with the same value of baryonic mass.

The figure is composed of three panels that correspond to the (a) mass, (b) radius, and (c) compactness. These results are then fitted by the following polynomial ansatz:

$$y = \sum_{n=1}^{m} a_n\, x^n, \quad m = 1,\ 3. \tag{6}$$

The relation between M_K and M_S showed almost linear behavior with deviations of at most a few percent. The relation R_K-R_S has a significantly more complicated shape and the fits with polynomials provide an accuracy of only the order of 10%. Per definition, the C_K-C_S relation has a similar accuracy. It shows a quasilinear behavior for small C_S (large R_S) values but strong deviations from the linear form in the opposite limit of large C_S (small R_S) values. Table IV summarizes the fit coefficients for the above relations, together with the corresponding values of $\chi^2_{\rm red}$.

B. Relating Keplerian frequency to static mass and radius

We now study the relation between the Keplerian frequency f_K of a CS and the gravitational mass and radius of the associated static star with same baryonic mass M_B. In the rigid-body Newtonian limit, the Keplerian frequency takes a very simple form, which originates from the balance between gravitational and centrifugal forces at the object's equator. The Keplerian frequency of a Newtonian sphere with mass M and

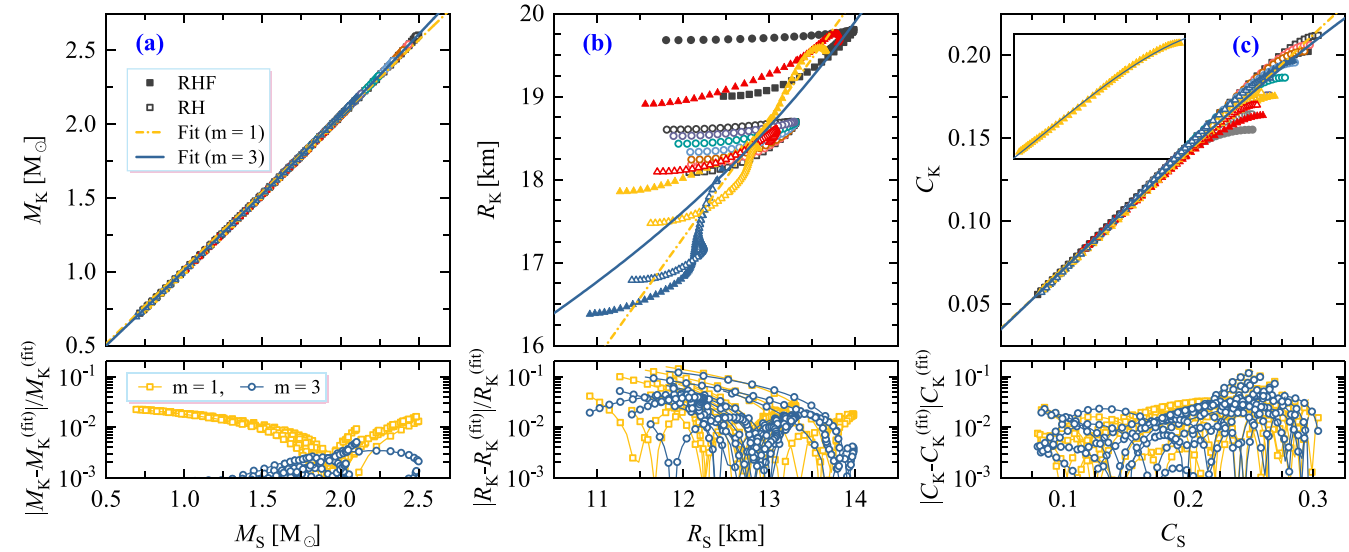

FIG. 12. The relations between mass, radius, and compactness of Keplerian CSs and their static counterparts which have the same baryonic mass M_B, i.e., the sequences are generated by varying M_B. (Top) Data for various EoS models together with the fitting curves. The result for a single EoS model fitted with a third-order polynomial is illustrated in the inset. (Bottom) Fractional errors between the fitting curves and numerical results.

TABLE IV. Estimated coefficients of the relations between the masses, radii, and compactness of Keplerian CSs and their static counterparts, for constant baryonic mass sequences. The corresponding reduced χ-squared ($\chi^2_{\rm red}$) values are given in the last column.

y	x	a_1	a_2	a_3	$\chi^2_{\rm red}$
$M_{\rm K}$	$M_{\rm S}$	1.02816×10^{0}			2.35621×10^{-4}
		9.97523×10^{-1}	6.52004×10^{-3}	4.79654×10^{-3}	7.19416×10^{-6}
$R_{\rm K}$	$R_{\rm S}$	1.44171×10^{0}			2.82323×10^{-1}
		3.61768×10^{0}	-3.12820×10^{-1}	1.11383×10^{-2}	2.20765×10^{-1}
$C_{\rm K}$	$C_{\rm S}$	7.07964×10^{-1}			1.98714×10^{-5}
		6.80281×10^{-1}	4.18057×10^{-1}	-1.25613×10^{0}	1.84240×10^{-5}

radius R is given by [81]

$$f_{\rm K}^{(\rm N)} = \frac{1}{2\pi}\sqrt{\frac{GM}{R^3}} = 1.8335\left(\frac{M}{M_\odot}\right)^{1/2}\left(\frac{10\,\text{km}}{R}\right)^{3/2}\text{kHz}. \quad (7)$$

Considering deformation and the dragging of local inertial frames within the general theory of relativity [107], the Keplerian frequency exhibits a complicated dependence on the global structure of a CS. To obtain the Keplerian frequency for a given EoS, it is generally necessary to calculate the equilibrium configurations within a self-consistent numerical framework, as discussed in the Appendix. Formula (7) is utilized to evaluate the general relativistic Keplerian frequency with the formula

$$f_{\rm K} = a\left(\frac{M_\tau}{M_\odot}\right)^{1/2}\left(\frac{10\,\text{km}}{R_\tau}\right)^{3/2}\text{kHz} = a\,C_\tau\,\text{kHz}, \quad (8)$$

where

$$C_\tau = \left(\frac{M_\tau}{M_\odot}\right)^{1/2}\left(\frac{10\,\text{km}}{R_\tau}\right)^{3/2}, \quad (9)$$

and τ denotes the configuration type, where $\tau = \text{S}$ for static configurations and $\tau = \text{K}$ for Keplerian ones.

In Fig. 13, we show the Keplerian frequency $f_{\rm K}$ plotted against the corresponding parameters of static stars, namely $(M_{\rm S}/M_\odot)^{1/2}(10\,\text{km}/R_{\rm S})^{3/2}$ for constant baryonic mass sequences in panel (a), and against themselves, $(M_{\rm K}/M_\odot)^{1/2}(10\,\text{km}/R_{\rm K})^{3/2}$, in panel (b). We perform linear fits and third-order extensions for each correlation according to

$$f_{\rm K} = \sum_{n=1}^{m} a_n\,(C_\tau)^n, \quad m = 1,\ 3. \quad (10)$$

Based on Fig. 13, it is apparent that a linear correlation is inadequate to fully capture the data, suggesting that a more complex or higher-order formula is necessary. In fact, as shown in the inset of Fig. 13, a third-order polynomial could well describe $f_{\rm K}$ for constant baryonic mass sequences, computed for a given EoS. We thus perform for each relation a third-order polynomial fit.

As depicted in Fig. 13, fitting the data with a third-order polynomial provides an accuracy of 5% in assessing the

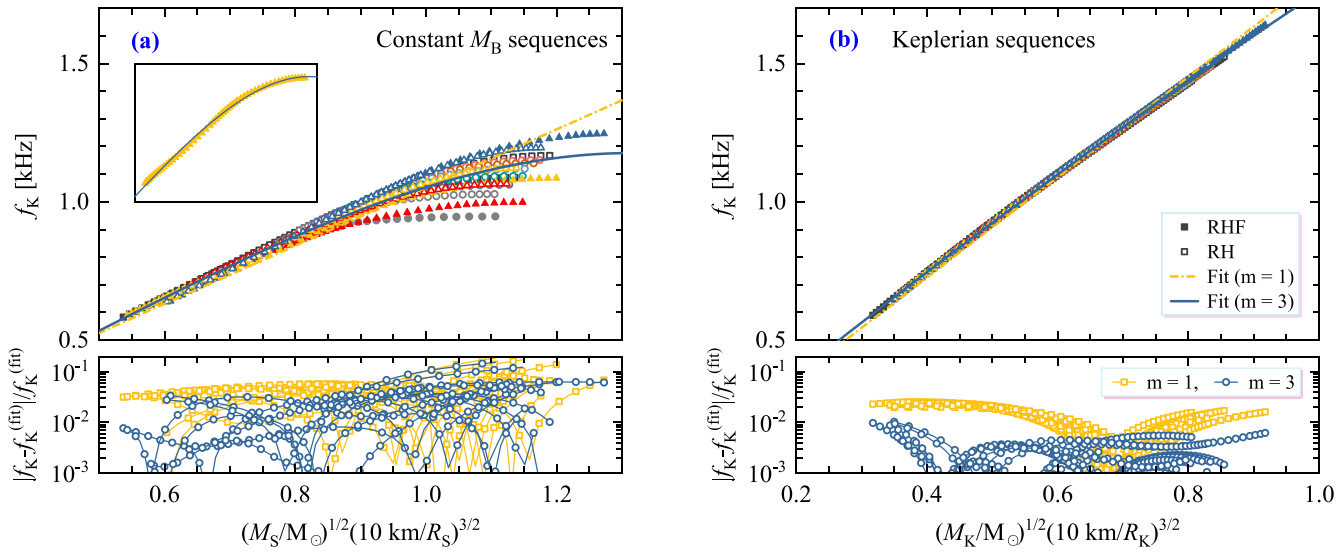

FIG. 13. (a) The Keplerian frequencies of CSs as a function of $C_{\rm S}$ [see Eq. (9)]. The Keplerian frequency and static mass and radius values are related by assuming that the static and Keplerian CS have the same fixed baryonic mass, i.e., the sequences are generated by varying $M_{\rm B}$. (b) Same as in (a), but as a function of $C_{\rm K}$ along the Keplerian sequence. (Top) Data from various EoS models and fitting curves as shown. The inset shows the result for a single EoS model using a third-order fitting polynomial. (Bottom) Fractional errors between the fitting curves and numerical results.

TABLE V. Estimated coefficients of the relations that involve the masses, radii, and frequencies of static and maximally (Keplerian) rotating CSs, for constant baryonic mass sequences. The corresponding reduced χ-squared ($\chi^2_{\rm red}$) values are given in the last column.

y	x	a_1	a_2	a_3	$\chi^2_{\rm red}$
$f_{\rm K}$	$C_{\rm S}$	1.05183×10^{0}			2.55674×10^{-3}
		7.95060×10^{-1}	8.34800×10^{-1}	-5.77261×10^{-1}	1.30980×10^{-3}
$f_{\rm K}$	$C_{\rm K}$	1.81576×10^{0}			1.56677×10^{-4}
		1.91746×10^{0}	-1.19466×10^{-1}	-3.83918×10^{-2}	9.29333×10^{-6}

Keplerian frequency of a CS using its static counterpart for constant baryonic mass sequences up to $0.9\,M^{\rm S}_{\rm max}$, where $M^{\rm S}_{\rm max}$ is the maximum mass of the nonrotating (static) configuration. Finally, the accuracy reaches 1% if one writes the Keplerian frequency of the star in terms of its mass and radius. The coefficients for each fitting curve are summarized in Table V.

C. Relations between gross properties of maximum-mass static and Keplerian configurations

As a follow-up to the previous subsection, we next will examine the relationship between gross properties (gravitational and baryonic mass, radius, and compactness) of the maximum-mass static and Keplerian configurations. Since for each EoS model, we have one datapoint relating these quantities to the static and maximally rotating configurations, it is necessary to incorporate additional EoS models to quantify and validate the universal relations. Thus, we consider: (i) Nucleonic CDF models proposed in Ref. [93], which are characterized by two nuclear matter parameters: the skewness $Q_{\rm sat}$ and the slope of the symmetry energy $L_{\rm sym}$. These models cover $2.0 \lesssim M_{\rm max} \lesssim 2.5\,M_\odot$ and $12 \lesssim R_{1.4} \lesssim 14.5$ km. (ii) Hyperonic CDF models proposed in Ref. [98], which are constructed by varying the values of parameters $L_{\rm sym}$ and $Q_{\rm sat}$ in the nucleonic sector and the couplings of hyperons in the SU(3) symmetric model. These models predict $2.0 \lesssim M_{\rm max} \lesssim 2.5\,M_\odot$ and $12.5 \lesssim R_{1.4} \lesssim 14.5$ km. (iii) Δ-admixed hyperonic CDF models for the EoS proposed in Ref. [93], which are constructed by varying the values of $L_{\rm sym}$ and $Q_{\rm sat}$ in the nucleonic sector and varying the strength of the Δ potential, while setting the couplings of hyperons according to the SU(6) symmetric model. The latter models lead to $2.0 \lesssim M_{\rm max} \lesssim 2.2\,M_\odot$ and $12 \lesssim R_{1.4} \lesssim 13.5$ km.

The correlations between the gross properties (baryonic and gravitational masses, radius, and compactness) of maximum-mass static and Keplerian configurations for each EoS model in our collection are shown in Fig. 14. We perform for each correlation a linear fit,

$$y = a\,x, \tag{11}$$

where the values of x and y correspond to quantities in the static and maximally rotating configurations, respectively, and are used to determine the linear fit for each correlation. The coefficient and its standard error related to each fit (a linear regression without an intercept term) can be found in Table VI. The uncertainty bounds that correspond to the standard deviation of the data from this regression coefficient are also estimated.

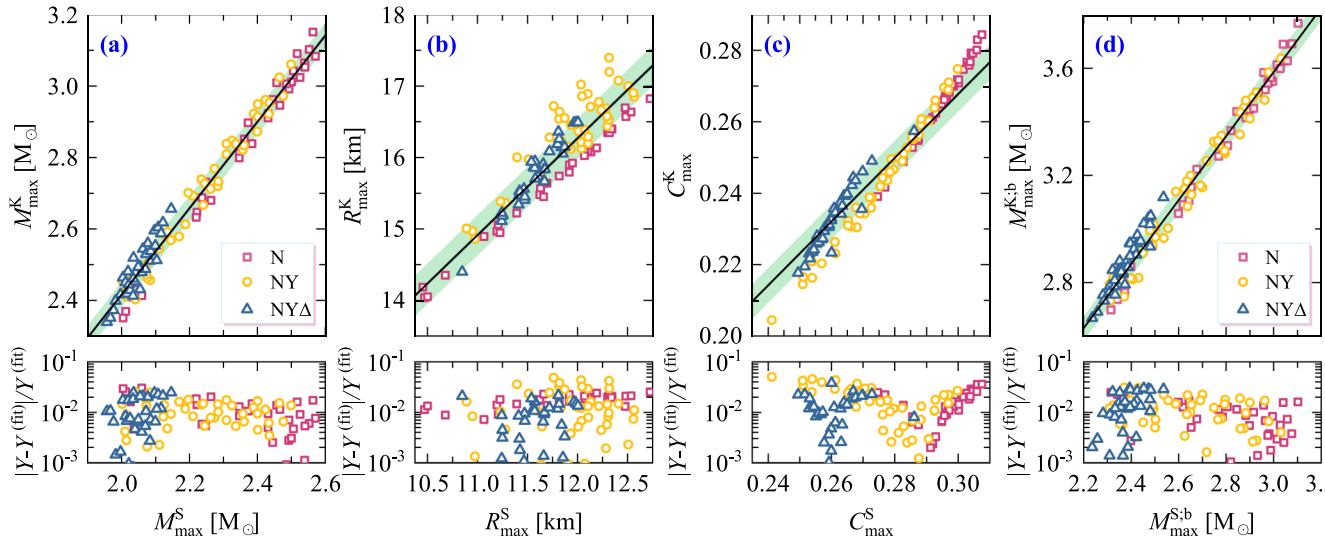

FIG. 14. The correlations between the gravitational (a) and baryonic (d) masses, radii (b), and compactness (c) of maximum-mass Keplerian and static stellar configurations. (Top) For each quantity the correlation for any EoS considered is represented by a dot and is approximated by a fitting line. The bands depict the 68.3% prediction intervals of the linear regressions. (Bottom) Fractional differences between the numerical results and the fitting lines.

TABLE VI. The values of the coefficient a for the linear relation between the parameters (maximum mass, radius, and compactness) of maximally rotating (Keplerian) and static stars. The values quoted in the parentheses refer to the standard error of this coefficient. The upper and lower bounds (error bars) quoted correspond to the standard deviation of the data from this regression coefficient.

y	x	a	$\chi^2_{\rm red}$
$M^{\rm K}_{\rm max}$	$M^{\rm S}_{\rm max}$	$1.20815\,(0.00147) \pm 0.01560$	1.15397×10^{-3}
$R^{\rm K}_{\rm max}$	$R^{\rm S}_{\rm max}$	$1.35578\,(0.00225) \pm 0.02305$	7.62623×10^{-2}
$C^{\rm K}_{\rm max}$	$C^{\rm S}_{\rm max}$	$0.89251\,(0.00164) \pm 0.01728$	2.25251×10^{-5}
$M^{\rm K;b}_{\rm max}$	$M^{\rm S;b}_{\rm max}$	$1.19522\,(0.00161) \pm 0.01725$	1.91463×10^{-3}

TABLE VII. The values of the coefficient a for the Keplerian frequency of maximally rotating stars in terms of their masses and radii, as well as those of the maximum-mass static stars. The values quoted in the parentheses refer to the standard error of this coefficient. The upper and lower bounds (error bars) quoted correspond to the standard deviation of the data from this regression coefficient.

y	x	a	$\chi^2_{\rm red}$
$f_{\rm K}$	$C^{\rm S;g}_{\rm max}$	$1.25106\,(0.00250) \pm 0.02638$	9.16179×10^{-4}
$f_{\rm K}$	$C^{\rm S;b}_{\rm max}$	$1.15339\,(0.00190) \pm 0.02010$	6.22013×10^{-4}
$f_{\rm K}$	$C^{\rm K;g}_{\rm max}$	$1.79396\,(0.00078) \pm 0.00824$	4.33169×10^{-5}
$f_{\rm K}$	$C^{\rm K;b}_{\rm max}$	$1.66183\,(0.00154) \pm 0.01632$	1.96817×10^{-4}

In this scenario, as shown in Fig. 14, the linear fit between masses ($M^{\rm S}_{\rm max}$, $M^{\rm K}_{\rm max}$) leads to a nearly perfect agreement which holds better than 3%. The deviations are by a factor of 2 larger for radii ($R^{\rm S}_{\rm max}$, $R^{\rm K}_{\rm max}$) and compactnesses ($C^{\rm S}_{\rm max}$, $C^{\rm K}_{\rm max}$). In addition, it is worth noting that in Fig. 14(b), the data calculated from purely nucleonic EoS models show an almost linear behavior, whereas those from heavy-baryons admixed EoS models are distributed somewhat randomly.

We also show in Fig. 14(d) the relationship between baryonic masses, where again, we observe an almost linear relation between static and Keplerian stars. This suggests the existence of a relation between the gravitational mass and baryonic mass for CSs in both static and Keplerian configurations.

Finally, we examine the relationships between the Keplerian frequency and the gross properties of both static and maximally rotating CSs, including the maximum gravitational mass, baryonic mass, and corresponding radius [65,73,81,107]. As in Eq. (8), we use the formula

$$f_{\rm K} = a\, C^{\tau}_{\rm max}\ {\rm kHz}, \tag{12}$$

where

$$C^{\tau}_{\rm max} = \left(\frac{M^{\tau}_{\rm max}}{M_\odot}\right)^{1/2} \left(\frac{10\,{\rm km}}{R^{\tau}_{\rm max}}\right)^{3/2}. \tag{13}$$

The symbol τ is used to indicate the form of the configuration, where τ can take on the values S; g and S; b for static configurations with gravitational and baryonic masses, respectively, and K; g and K; b for Keplerian configurations.

Our results are presented in Fig. 15. The maximum rotation frequency is an increasing function of the softness of an EoS, while the maximum mass decreases. Consequently, the data predicted by EoSs featuring heavy baryons are located mainly at the bottom-left part of each figure. As expected, we find a strong correlation between the Keplerian frequency $f_{\rm K}$ and the mass-radius combination $C^{\rm K}_{\rm max}$ of the rotating configuration defined in Eq. (13); this correlation holds an accuracy better than 2%. The mass-radius combination $C^{\rm S}_{\rm max}$ of a static configuration could still be used to assess the Keplerian frequency $f_{\rm K}$ with an accuracy up to 6%. The coefficients for each fitting are summarized in Table VII.

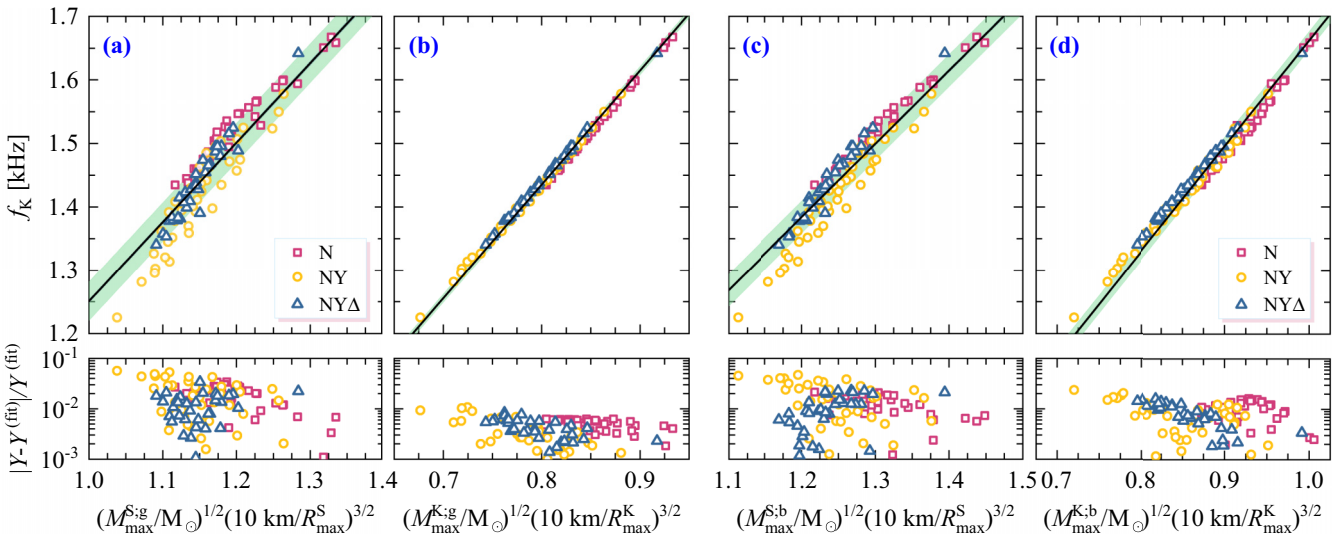

FIG. 15. The correlation between the Keplerian frequency of maximally rotating CS and $C^{\tau}_{\rm max}$, see Eq. (13), where (a) and (b) use gravitational static and Keplerian masses respectively, whereas (c) and (d) their baryonic counterparts instead. (Top) For each quantity the correlation for any EoS considered is represented by a dot and is approximated by a fitting line. The bands depict the 68.3% prediction intervals of the linear regressions. (Bottom) Fractional differences between the numerical results and fitting lines.

V. CONCLUSIONS

In this work, we investigated universal relations for CSs containing heavy baryons. We constructed EoS models of dense matter with hyperons and Δ resonances within the covariant density functional theory. To construct these models, the couplings in the nucleonic sector were calibrated by nuclear phenomenology. The couplings of heavy baryons in the scalar-meson sector were determined by fitting their potentials at symmetric nuclear matter. The vector meson couplings were determined using the spin-flavor symmetries of the quark model and its breaking. The resulting EoS models are constructed to be consistent with available constraints from nuclear physics experiments and observations of CSs, specifically, radii and masses inferred by the modeling of the NICER observations. The models predict maximum-mass stars and corresponding radius values that are within the ranges of $2.0 \lesssim M_{\max} \lesssim 2.5 M_{\odot}$ and $11.5 \lesssim R_{1.4} \lesssim 14.5$ km.

We first studied the measurable global properties of CSs including mass, radius, tidal deformability, moment of inertia, and quadrupole moment for isolated stars. We have demonstrated that the inclusion of heavy baryons in CSs does not affect the universal properties of the $\bar{I}$-Λ-$\bar{Q}$ relations for static configurations (within the slow-rotation approximation) or the $\bar{I}$-C-$\bar{Q}$ relations for constant spin sequences, as we move from static to rapidly rotating configurations. The former relations are found to be accurate up to 1%, while the latter ones have a larger relative error of the order of 8% (except for the $\bar{I}$-$\bar{Q}$ pair). We further argue that the $\bar{I}$-C-$\bar{Q}$ relation may hold for maximally rotating (Keplerian) configurations since the maximum spin parameter $\chi_{\max} = 0.68 \pm 0.04$ remains constant within 6% for stars within the mass range of interest. The radial dependence of the integrands entering the calculations of mass, the moment of inertia, quadrupole moment, and tidal deformability in the Newtonian limit were examined. It was shown that the presence of heavy baryons breaks the similarity of the radial profiles, rendering the physical origin of these relations more complex.

We next investigated the correlations between the properties of maximally rotating (Keplerian) stars and their nonrotating counterparts for sequences with the same baryonic mass. It was found that for sequences with constant baryonic mass, a remarkably tight correlation exists between their masses, with an accuracy of better than 0.5%. The Keplerian frequency of a maximally rotating star can be estimated with an accuracy of approximately 10% and 2% using the mass and radius of both the static and rotating stellar configurations, respectively. Correlations between the global properties of static and rotating maximum-mass configurations were also studied. We found that the presence of a significant number of heavy baryons results in slight variations in these relations compared to those obtained for CSs composed solely of nucleonic matter.

In conclusion, this work presents a study on the universal relations for CSs that contain heavy baryons. Our derived relations are updated versions of those already present in the literature as applied to EoS collection with a focus on heavy baryon degrees of freedom. The obtained relations can be used to make EoS-insensitive estimates of CS properties using, for example, the GW data. Future astronomical observations in combination with these relations can be used to improve and expand our understanding of the EoS of dense matter.

ACKNOWLEDGMENTS

J.J.L. is supported by the National Natural Science Foundation of China (Grant No. 12105232), the Venture & Innovation Support Program for Chongqing Overseas Returnees (Grant No. CX2021007), and by the "Fundamental Research Funds for the Central Universities" (Grant No. SWU-020021). A.S. is funded by Deutsche Forschungsgemeinschaft Grant No. SE 1836/5-2 and the Polish NCN Grant No. 2020/37/B/ST9/01937 at Wrocław University. F.W. acknowledges support provided by the U.S. National Science Foundation under Grant No. PHY-2012152.

APPENDIX: EQUILIBRIUM MODELS FOR CSS

In this Appendix, we briefly specify the relevant equations and methods that are used to compute the various integral parameters of static and rotating stars within the general theory of relativity. The stellar matter is assumed to be a perfect fluid whose energy-momentum tensor can be written as

$$T_{\mu\nu} = (\varepsilon + P) u_\mu u_\nu + P g_{\mu\nu}, \tag{A1}$$

where ε and P are the energy density and pressure of matter, respectively. The quantity u_μ represents the four-velocity of the matter and $g_{\mu\nu}$ is the metric tensor.

1. Static models

In the case of static stars, the metric is spherical symmetrical and is given by

$$ds^2 = -e^{2\nu(r)} dt^2 + e^{2\lambda(r)} dr^2 + r^2 (d\theta^2 + \sin^2\theta \, d\varphi^2), \tag{A2}$$

where $\nu(r)$ and $\lambda(r)$ are metric functions which depend on the radial coordinate r.

The static solutions of Einstein's equations are given by the Tolman-Oppenheimer-Volkoff (TOV) equations [108,109]

$$\frac{dm(r)}{dr} = 4\pi r^2 \varepsilon, \tag{A3a}$$

$$\frac{dP(r)}{dr} = -\frac{(\varepsilon + P)(m + 4\pi r^3 P)}{r^2 \left(1 - \frac{2m}{r}\right)}, \tag{A3b}$$

where $m(r)$ is the mass enclosed in a mass shell at distance r from the center of the star. Equations (A3a) and (A3b) are numerically integrated over the radial coordinate r from $r = 0$ to $r = R$, where radius R is the radial distance at which the pressure P becomes zero.

The tidal deformability, λ, determines how easily an object can be deformed due to an external tidal field [110,111]. It is given via the dimensionless tidal Love number k_2 and the star's radius, R, as $\lambda = 2/3 k_2 R^5$, where

$$k_2 = \tfrac{8}{5} C^5 (1 - 2C)^2 [2 + 2C(y_R - 1) - y_R] \times \{6C[2 - y_R + C(5y_R - 8)]$$

$$+\ 4C^3[13-11y_R+C(3y_R-2)+2C^2(1+y_R)]$$
$$+\ 3(1-2C)^2[2-y_R+2C(y_R-1)]\ln(1-2C)\}^{-1}. \tag{A4}$$

The quantity $C=M/R$ is the dimensionless compactness of the star, and $y_R=y(R)$ is extracted from the solution of

$$\frac{dy(r)}{dr}=-\frac{1}{r}y^2-\frac{1}{r}F_1 y-rF_2, \tag{A5}$$

where

$$F_1=\frac{1-4\pi r^2(\varepsilon-P)}{\left(1-\frac{2m}{r}\right)}, \tag{A6a}$$

$$F_2=\frac{4\pi}{\left(1-\frac{2m}{r}\right)}\left(5\varepsilon+9P+\frac{\varepsilon+P}{c_s^2}-\frac{6}{4\pi r^2}\right)-4\left[\frac{(m+4\pi r^3P)}{r^2\left(1-\frac{2m}{r}\right)}\right]^2. \tag{A6b}$$

Here, $c_s^2=dP/d\varepsilon$ represents the square of the speed of sound. Equation (A5) has to be integrated simultaneously with the TOV Eqs. (A3a) and (A3b) with a boundary value $y(0)=2$. It is more convenient to work with the dimensionless Λ, which is related to the Love number k_2 and the compactness parameter through

$$\Lambda=\tfrac{2}{3}\,k_2\,C^{-5}. \tag{A7}$$

A sequence of stars, each with its mass, radius, tidal deformability, etc., can be generated by varying the central density ε_c or pressure P_c.

2. Rotating models

Highly accurate numerical methods for computing the properties of rotating stars have been developed [102,112–115]. Equilibrium configurations of rotating stars can be computed using the publicly available RNS [113,116] and LORENE/ROTSTAR [114,117] codes.

We employed the RNS code [118] to obtain the results for rotating stars reported below. It solves the Einstein field equations for an axisymmetric and stationary space-time described by the metric

$$ds^2=-e^{\gamma+\rho}dt^2+e^{2\alpha}(dr^2+r^2d\theta^2)+e^{\gamma-\rho}r^2\sin^2\theta\,(d\phi-\omega dt)^2, \tag{A8}$$

where γ, ρ, α, and ω are metric potentials that depend on the radial coordinates r and the polar angle θ.

Using the RNS code, we computed the mass, radius, moment of inertia, and quadrupole moment of rotating star for a specified central density. Our results take into account the correction for the quadrupole moment Q given in Refs. [42,119].

Dimensionless quantities for the moment of inertia and the quadrupole moment can be defined as follows:

$$\bar{I}=\frac{I}{M^3}\quad\text{and}\quad\bar{Q}=-\frac{Q}{M^3\chi^2}, \tag{A9}$$

where M is the gravitational mass, $\chi=J/M^2$ represents the dimensionless spin parameter, and J is the angular momentum. The oblate shape of a rotating CS is approximately universal and can be described by a function of the equatorial compactness $C_{\rm eq}=M/R_{\rm eq}$ (where $R_{\rm eq}$ is the radius of the star measured at the equator) and the angular velocity [120]. In this work, we will use C to refer to the equatorial compactness of rotating stars.

Finally, for completeness, we quote the equation for the general relativistic Keplerian frequency $f_{\rm K}$ for a test particle moving along the orbit with semimajor axis $a_{\rm K}$ around a body with mass M,

$$f_{\rm K}=\left(\frac{GM}{a_{\rm K}^3}\right)^{1/2}\left[1-\left(\frac{3GM}{c^2a_{\rm K}}\right)(1-\epsilon^2)\right], \tag{A10}$$

where ϵ is the eccentricity of the orbit. It reduces to Eq. (8) by considering a test particle moving along the equatorial circumference of the Keplerian star of mass $M_{\rm K}$.

[1] J. M. Lattimer, The nuclear equation of state and neutron star masses, Annu. Rev. Nucl. Part. Sci. **62**, 485 (2012).
[2] D. Chatterjee and I. Vidaña, Do hyperons exist in the interior of neutron stars?, Eur. Phys. J. A **52**, 29 (2016).
[3] J. M. Lattimer and M. Prakash, The equation of state of hot, dense matter and neutron stars, Phys. Rep. **621**, 127 (2016).
[4] M. Oertel, M. Hempel, T. Klähn, and S. Typel, Equations of state for supernovae and compact stars, Rev. Mod. Phys. **89**, 015007 (2017).
[5] F. Özel and P. Freire, Masses, radii, and the equation of state of neutron stars, Annu. Rev. Astron. Astrophys. **54**, 401 (2016).
[6] G. Baym, T. Hatsuda, T. Kojo, P. D. Powell, Y. Song, and T. Takatsuka, From hadrons to quarks in neutron stars: A review, Rep. Prog. Phys. **81**, 056902 (2018).
[7] A. Sedrakian and J. W. Clark, Superfluidity in nuclear systems and neutron stars, Eur. Phys. J. A **55**, 167 (2019).
[8] L. Baiotti, Gravitational waves from neutron star mergers and their relation to the nuclear equation of state, Prog. Part. Nucl. Phys. **109**, 103714 (2019).
[9] L. Tolos and L. Fabbietti, Strangeness in nuclei and neutron stars, Prog. Part. Nucl. Phys. **112**, 103770 (2020).
[10] D. Logoteta, Hyperons in neutron stars, Universe **7**, 408 (2021).
[11] G. F. Burgio, H. J. Schulze, I. Vidana, and J. B. Wei, Neutron stars and the nuclear equation of state, Prog. Part. Nucl. Phys. **120**, 103879 (2021).
[12] J. M. Lattimer, Neutron stars and the nuclear matter equation of state, Annu. Rev. Nucl. Part. Sci. **71**, 433 (2021).
[13] A. Sedrakian, J. J. Li, and F. Weber, Heavy baryons in compact stars, Prog. Part. Nucl. Phys. **131**, 104041 (2023).
[14] B. P. Abbott, R. Abbott, T. D. Abbott, F. Acernese, K. Ackley *et al.*, Multi-messenger observations of a binary neutron star merger, Astrophys. J. Lett. **848**, L12 (2017).

[15] B. P. Abbott, R. Abbott, T. D. Abbott, F. Acernese, K. Ackley *et al.* (LIGO Scientific, Virgo Collaboration), GW170817: Observation of Gravitational Waves from a Binary Neutron Star Inspiral, Phys. Rev. Lett. **119**, 161101 (2017).
[16] E. Annala, T. Gorda, A. Kurkela, and A. Vuorinen, Gravitational-Wave Constraints on the Neutron-Star-Matter Equation of State, Phys. Rev. Lett. **120**, 172703 (2018).
[17] F. J. Fattoyev, J. Piekarewicz, and C. J. Horowitz, Neutron Skins and Neutron Stars in the Multimessenger Era, Phys. Rev. Lett. **120**, 172702 (2018).
[18] A. Bauswein, O. Just, H.-T. Janka, and N. Stergioulas, Neutron-star radius constraints from GW170817 and future detections, Astrophys. J. Lett. **850**, L34 (2017).
[19] E. R. Most, L. R. Weih, L. Rezzolla, and J. Schaffner-Bielich, New Constraints on Radii and Tidal Deformabilities of Neutron Stars from GW170817, Phys. Rev. Lett. **120**, 261103 (2018).
[20] S. De, D. Finstad, J. M. Lattimer, D. A. Brown, E. Berger, and C. M. Biwer, Tidal Deformabilities and Radii of Neutron Stars from the Observation of GW170817, Phys. Rev. Lett. **121**, 091102 (2018).
[21] M. W. Coughlin, T. Dietrichand, Z. Doctor, D. Kasen, S. Coughlin *et al.*, Constraints on the neutron star equation of state from AT2017gfo using radiative transfer simulations, Mon. Not. Roy. Astron. Soc. **480**, 3871 (2018).
[22] J. J. Li and A. Sedrakian, Implications from GW170817 for Δ-isobar admixed hypernuclear compact stars, Astrophys. J. Lett. **874**, L22 (2019).
[23] D. Psaltis, F. Özel, and D. Chakrabarty, Prospects for measuring neutron-star masses and radii with x-ray pulse profile modeling, Astrophys. J. **787**, 136 (2014).
[24] T. E. Riley, A. L. Watts, S. Bogdanov, P. S. Ray, R. M. Ludlam *et al.*, A NICER view of PSR J0030+0451: Millisecond pulsar parameter estimation, Astrophys. J. Lett. **887**, L21 (2019).
[25] M. C. Miller, F. K. Lamb, A. J. Dittmann, S. Bogdanov, Z. Arzoumanian *et al.*, PSR J0030+0451 mass and radius from NICER data and implications for the properties of neutron star matter, Astrophys. J. Lett. **887**, L24 (2019).
[26] T. E. Riley, A. L. Watts, P. S. Ray, S. Bogdanov, S. Guillot *et al.*, A NICER view of the massive pulsar PSR J0740+6620 informed by radio timing and XMM-Newton spectroscopy, Astrophys. J. Lett. **918**, L27 (2021).
[27] M. C. Miller, F. K. Lamb, A. J. Dittmann, S. Bogdanov, Z. Arzoumanian *et al.*, The radius of PSR J0740+6620 from NICER and XMM-Newton data, Astrophys. J. Lett. **918**, L28 (2021).
[28] M. Fasano, T. Abdelsalhin, A. Maselli, and V. Ferrari, Constraining the Neutron Star Equation of State Using Multiband Independent Measurements of Radii and Tidal Deformabilities, Phys. Rev. Lett. **123**, 141101 (2019).
[29] I. Legred, K. Chatziioannou, R. Essick, S. Han, and P. Landry, Impact of the PSR J0740+6620 radius constraint on the properties of high-density matter, Phys. Rev. D **104**, 063003 (2021).
[30] G. Raaijmakers, S. K. Greif, K. Hebeler, T. Hinderer, S. Nissanke *et al.*, Constraints on the dense matter equation of state and neutron star properties from NICER's mass-radius estimate of PSR J0740+6620 and multimessenger observations, Astrophys. J. Lett. **918**, L29 (2021).
[31] S.-P. Tang, J.-L. Jiang, M.-Z. Han, Y.-Z. Fan, and D.-M. Wei, Constraints on the phase transition and nuclear symmetry parameters from PSR J0740+6620 and multimessenger data of other neutron stars, Phys. Rev. D **104**, 063032 (2021).
[32] N.-B. Zhang and B.-A. Li, Impact of NICER's radius measurement of PSR J0740+6620 on nuclear symmetry energy at suprasaturation densities, Astrophys. J. **921**, 111 (2021).
[33] J. J. Li, A. Sedrakian, and M. Alford, Relativistic hybrid stars in light of the NICER PSR J0740+6620 radius measurement, Phys. Rev. D **104**, L121302 (2021).
[34] J.-E. Christian and J. Schaffner-Bielich, Confirming the existence of twin stars in a NICER way, Astrophys. J. **935**, 122 (2022).
[35] K. Yagi and N. Yunes, I-Love-Q: Unexpected universal relations for neutron stars and quark stars, Science **341**, 365 (2013).
[36] K. Yagi and N. Yunes, I-Love-Q relations in neutron stars and their applications to astrophysics, gravitational waves and fundamental physics, Phys. Rev. D **88**, 023009 (2013).
[37] D. D. Doneva, S. S. Yazadjiev, N. Stergioulas, and K. D. Kokkotas, Breakdown of I-Love-Q universality in rapidly rotating relativistic stars, Astrophys. J. Lett. **781**, L6 (2013).
[38] A. Maselli, V. Cardoso, V. Ferrari, L. Gualtieri, and P. Pani, Equation-of-state-independent relations in neutron stars, Phys. Rev. D **88**, 023007 (2013).
[39] M. Bauböck, E. Berti, D. Psaltis, and F. Özel, Relations between neutron-star parameters in the Hartle-Thorne approximation, Astrophys. J. **777**, 68 (2013).
[40] B. Haskell, R. Ciolfi, F. Pannarale, and L. Rezzolla, On the universality of I-Love-Q relations in magnetized neutron stars, Mon. Not. Roy. Astron. Soc. **438**, L71 (2014).
[41] G. Pappas and T. A. Apostolatos, Effectively Universal Behavior of Rotating Neutron Stars in General Relativity Makes Them Even Simpler than Their Newtonian Counterparts, Phys. Rev. Lett. **112**, 121101 (2014).
[42] K. Yagi, K. Kyutoku, G. Pappas, N. Yunes, and T. A. Apostolatos, Effective no-hair relations for neutron stars and quark stars: Relativistic results, Phys. Rev. D **89**, 124013 (2014).
[43] S. Chakrabarti, T. Delsate, N. Gürlebeck, and J. Steinhoff, I-Q Relation for Rapidly Rotating Neutron Stars, Phys. Rev. Lett. **112**, 201102 (2014).
[44] G. Martinon, A. Maselli, L. Gualtieri, and V. Ferrari, Rotating protoneutron stars: Spin evolution, maximum mass, and I-Love-Q relations, Phys. Rev. D **90**, 064026 (2014).
[45] A. W. Steiner, J. M. Lattimer, and E. F. Brown, Neutron star radii, universal relations, and the role of prior distributions, Eur. Phys. J. A **52**, 18 (2016).
[46] F. Cipolletta, C. Cherubini, S. Filippi, J. A. Rueda, and R. Ruffini, Fast rotating neutron stars with realistic nuclear matter equation of state, Phys. Rev. D **92**, 023007 (2015).
[47] C. Breu and L. Rezzolla, Maximum mass, moment of inertia and compactness of relativistic stars, Mon. Not. R. Astron. Soc. **459**, 646 (2016).
[48] K. V. Staykov, D. D. Doneva, and S. S. Yazadjiev, Moment-of-inertia–compactness universal relations in scalar-tensor theories and $\mathcal{R}^2$ gravity, Phys. Rev. D **93**, 084010 (2016).
[49] K. Yagi and N. Yunes, Binary Love relations, Class. Quantum Grav. **33**, 13LT01 (2016).
[50] D. D. Doneva and S. S. Yazadjiev, Rapidly rotating neutron stars with a massive scalar field—structure and universal relations, J. Cosmol. Astropart. Phys. 11 (2016) 019.

[51] V. Paschalidis, K. Yagi, D. Alvarez-Castillo, D. B. Blaschke, and A. Sedrakian, Implications from GW170817 and I-Love-Q relations for relativistic hybrid stars, Phys. Rev. D **97**, 084038 (2018).
[52] H. O. Silva and N. Yunes, I-Love-Q to the extreme, Class. Quantum Grav. **35**, 015005 (2018).
[53] J. Gagnon-Bischoff, S. R. Green, P. Landry, and N. Ortiz, Extended I-Love relations for slowly rotating neutron stars, Phys. Rev. D **97**, 064042 (2018).
[54] M. Marques, M. Oertel, M. Hempel, and J. Novak, New temperature dependent hyperonic equation of state: Application to rotating neutron star models and *I*-*Q* relations, Phys. Rev. C **96**, 045806 (2017).
[55] J. B. Wei, A. Figura, G. F. Burgio, H. Chen, and H. J. Schulze, Neutron star universal relations with microscopic equations of state, J. Phys. G: Nucl. Part. Phys. **46**, 034001 (2019).
[56] S. S. Lenka, P. Char, and S. Banik, Properties of massive rotating protoneutron stars with hyperons: Structure and universality, J. Phys. G: Nucl. Part. Phys. **46**, 105201 (2019).
[57] Y. Lim, J. W. Holt, and R. J. Stahulak, Predicting the moment of inertia of pulsar J0737-3039A from Bayesian modeling of the nuclear equation of state, Phys. Rev. C **100**, 035802 (2019).
[58] J. R. Stone, V. Dexheimer, P. A. M. Guichon, A. W. Thomas, and S. Typel, Equation of state of hot dense hyperonic matter in the quark–meson-coupling (QMC-A) model, Mon. Not. Roy. Astron. Soc. **502**, 3476 (2021).
[59] R. Riahi, S. Z. Kalantari, and J. A. Rueda, Universal relations for the Keplerian sequence of rotating neutron stars, Phys. Rev. D **99**, 043004 (2019).
[60] B. Kumar and P. Landry, Inferring neutron star properties from GW170817 with universal relations, Phys. Rev. D **99**, 123026 (2019).
[61] D.-H. Wen, B.-A. Li, H.-Y. Chen, and N.-B. Zhang, GW170817 implications on the frequency and damping time of f-mode oscillations of neutron stars, Phys. Rev. C **99**, 045806 (2019).
[62] N. Jiang and K. Yagi, Analytic I-Love-C relations for realistic neutron stars, Phys. Rev. D **101**, 124006 (2020).
[63] W. Sun, D. Wen, and J. Wang, New quasi-universal relations for static and rapid rotating neutron stars, Phys. Rev. D **102**, 023039 (2020).
[64] A. R. Raduta, M. Oertel, and A. Sedrakian, Proto-neutron stars with heavy baryons and universal relations, Mon. Not. Roy. Astron. Soc. **499**, 914 (2020).
[65] P. S. Koliogiannis and C. C. Moustakidis, Effects of the equation of state on the bulk properties of maximally-rotating neutron stars, Phys. Rev. C **101**, 015805 (2020).
[66] D. A. Godzieba, R. Gamba, D. Radice, and S. Bernuzzi, Updated universal relations for tidal deformabilities of neutron stars from phenomenological equations of state, Phys. Rev. D **103**, 063036 (2021).
[67] V. Nedora, S. Bernuzzi, D. Radice, B. Daszuta, A. Endrizzi *et al.*, Numerical relativity simulations of the neutron star merger GW170817: Long-term remnant evolutions, winds, remnant disks, and nucleosynthesis, Astrophys. J. **906**, 98 (2021).
[68] S. Khadkikar, A. R. Raduta, M. Oertel, and A. Sedrakian, Maximum mass of compact stars from gravitational wave events with finite-temperature equations of state, Phys. Rev. C **103**, 055811 (2021).
[69] J. A. Saes and R. F. P. Mendes, Equation-of-state-insensitive measure of neutron star stiffness, Phys. Rev. D **106**, 043027 (2022).
[70] E. Annala, T. Gorda, E. Katerini, A. Kurkela, J. Nättilä, V. Paschalidis, and A. Vuorinen, Multimessenger Constraints for Ultradense Matter, Phys. Rev. X **12**, 011058 (2022).
[71] V. I. Danchev and D. D. Doneva, Constraining the equation of state in modified gravity via universal relations, Phys. Rev. D **103**, 024049 (2021).
[72] H.-J. Kuan, C. J. Krüger, A. G. Suvorov, and K. D. Kokkotas, Constraining equation-of-state groups from g-mode asteroseismology, Mon. Not. Roy. Astron. Soc. **513**, 4045 (2022).
[73] A. Konstantinou and S. M. Morsink, Universal relations for the increase in the mass and radius of a rotating neutron star, Astrophys. J. **934**, 139 (2022).
[74] S. Wang, C. Wang, and H. Tong, Exploring universal characteristics of neutron star matter with relativistic *ab initio* equations of state, Phys. Rev. C **106**, 045804 (2022).
[75] N. K. Largani, T. Fischer, A. Sedrakian, M. Cierniak, D. E. Alvarez-Castillo, and D. B. Blaschke, Universal relations for rapidly rotating cold and hot hybrid stars, Mon. Not. Roy. Astron. Soc. **515**, 3539 (2022).
[76] T. Zhao and J. M. Lattimer, Universal relations for neutron star f-mode and g-mode oscillations, Phys. Rev. D **106**, 123002 (2022).
[77] J. Bretz, K. Yagi, and N. Yunes, Four-hair relations for differentially rotating neutron stars in the weak-field limit, Phys. Rev. D **92**, 083009 (2015).
[78] J. Soldateschi, N. Bucciantini, and L. Del Zanna, Quasi-universality of the magnetic deformation of neutron stars in general relativity and beyond, Astron. Astrophys. **654**, 3684 (2021).
[79] K. Yagi and N. Yunes, Approximate universal relations for neutron stars and quark stars, Phys. Rep. **681**, 1 (2017).
[80] M. Bejger and P. Haensel, Moments of inertia for neutron and strange stars: Limits derived for the Crab pulsar, Astron. Astrophys. **396**, 917 (2002).
[81] J. M. Lattimer and M. Prakash, The physics of neutron stars, Science **304**, 536 (2004).
[82] M. Urbanec, J. C. Miller, and Z. Stuchlik, Quadrupole moments of rotating neutron stars and strange stars, Mon. Not. Roy. Astron. Soc. **433**, 1903 (2013).
[83] J. J. Li, A. Sedrakian, and F. Weber, Competition between delta isobars and hyperons and properties of compact stars, Phys. Lett. B **783**, 234 (2018).
[84] J. J. Li and A. Sedrakian, Constraining compact star properties with nuclear saturation parameters, Phys. Rev. C **100**, 015809 (2019).
[85] A. Sedrakian, F. Weber, and J. J. Li, Confronting GW190814 with hyperonization in dense matter and hypernuclear compact stars, Phys. Rev. D **102**, 041301(R) (2020).
[86] A. Sedrakian, Light clusters in dilute heavy-baryon admixed nuclear matter, Eur. Phys. J. A **56**, 258 (2020).
[87] A. Sedrakian and A. Harutyunyan, Delta-resonances and hyperons in proto-neutron stars and merger remnants, Eur. Phys. J. A **58**, 137 (2022).
[88] D. Adhikari, H. Albataineh, D. Androic, K. Aniol, D. S. Armstrong *et al.* (PREX Collaboration), Accurate Determination of the Neutron Skin Thickness of ^{208}Pb through Parity-Violation in Electron Scattering, Phys. Rev. Lett. **126**, 172502 (2021).

[89] B. T. Reed, F. J. Fattoyev, C. J. Horowitz, and J. Piekarewicz, Implications of PREX-2 on the Equation of State of Neutron-Rich Matter, Phys. Rev. Lett. **126**, 172503 (2021).
[90] P.-G. Reinhard, X. Roca-Maza, and W. Nazarewicz, Information Content of the Parity-Violating Asymmetry in ^{208}Pb, Phys. Rev. Lett. **127**, 232501 (2021).
[91] R. Essick, I. Tews, P. Landry, and A. Schwenk, Astrophysical Constraints on the Symmetry Energy and the Neutron Skin of ^{208}Pb with Minimal Modeling Assumptions, Phys. Rev. Lett. **127**, 192701 (2021).
[92] G. Malfatti, M. G. Orsaria, I. F. Ranea-Sandoval, G. A. Contrera, and F. Weber, Delta baryons and diquark formation in the cores of neutron stars, Phys. Rev. D **102**, 063008 (2020).
[93] J. J. Li, A. Sedrakian, and F. Weber, Rapidly rotating Δ-resonance-admixed hypernuclear compact stars, Phys. Lett. B **810**, 135812 (2020).
[94] J. J. Li, W. H. Long, and A. Sedrakian, Hypernuclear stars from relativistic Hartree-Fock density functional theory, Eur. Phys. J. A **54**, 133 (2018).
[95] R. Abbott Jr., T. D. Abbott, S. Abraham, F. Acernese, K. Ackley *et al.* (LIGO Scientific, Virgo Collaboration), GW190814: Gravitational waves from the coalescence of a 23 solar mass black hole with a 2.6 solar mass compact object, Astrophys. J. Lett. **896**, L44 (2020).
[96] W. H. Long, H. Sagawa, J. Meng, and N. Van Giai, Evolution of nuclear shell structure due to the pion exchange potential, Europhys. Lett. **82**, 12001 (2008).
[97] G. A. Lalazissis, T. Niksic, D. Vretenar, and P. Ring, New relativistic mean-field interaction with density-dependent meson-nucleon couplings, Phys. Rev. C **71**, 024312 (2005).
[98] H. R. Fu, J. J. Li, A. Sedrakian, and F. Weber, Massive relativistic compact stars from SU(3) symmetric quark models, Phys. Lett. B **834**, 137470 (2022).
[99] A. R. Raduta, Δ-admixed neutron stars: Spinodal instabilities and dUrca processes, Phys. Lett. B **814**, 136070 (2021).
[100] S. Postnikov, M. Prakash, and J. M. Lattimer, Tidal Love numbers of neutron and self-bound quark stars, Phys. Rev. D **82**, 024016 (2010).
[101] K.-W. Lo and L.-M. Lin, The spin parameter of uniformly rotating compact stars, Astrophys. J. **728**, 12 (2011).
[102] G. B. Cook, S. L. Shapiro, and S. A. Teukolsky, Rapidly rotating polytropes in general relativity, Astrophys. J. **422**, 227 (1994).
[103] P. Haensel, M. Salgado, and S. Bonazzola, Equation of state of dense matter and maximum rotation frequency of neutron stars, Astron. Astrophys. **296**, 745 (1995).
[104] Y. H. Sham, T. K. Chan, L. M. Lin, and P. T. Leung, Unveiling the universality of I-Love-Q relations, Astrophys. J. **798**, 121 (2015).
[105] N. Andersson and K. D. Kokkotas, The r-mode instability in rotating neutron stars, Int. J. Mod. Phys. D **10**, 381 (2001).
[106] E. L. Bratton, Z. Lin, F. Weber, M. G. Orsaria, I. F. Ranea-Sandoval, and N. Saavedra, Gravitational-wave instabilities in rotating compact stars, Galaxies **10**, 94 (2022).
[107] P. Haensel, J. L. Zdunik, M. Bejger, and J. M. Lattimer, Keplerian frequency of uniformly rotating neutron stars and strange stars, Astron. Astrophys. **502**, 605 (2009).
[108] R. C. Tolman, Static solutions of Einstein's field equations for spheres of fluid, Phys. Rev. **55**, 364 (1939).
[109] J. R. Oppenheimer and G. M. Volkoff, On massive neutron cores, Phys. Rev. **55**, 374 (1939).
[110] T. Hinderer, Tidal Love numbers of neutron stars, Astrophys. J. **677**, 1216 (2008).
[111] T. Binnington and E. Poisson, Relativistic theory of tidal Love numbers, Phys. Rev. D **80**, 084018 (2009).
[112] H. Komatsu, Y. Eriguchi, and I. Hachisu, Rapidly rotating general relativistic stars. I - Numerical method and its application to uniformly rotating polytropes, Mon. Not. R. Astron. Soc. **237**, 355 (1989).
[113] N. Stergioulas and J. L. Friedman, Comparing models of rapidly rotating relativistic stars constructed by two numerical methods, Astrophys. J. **444**, 306 (1995).
[114] S. Bonazzola, E. Gourgoulhon, M. Salgado, and J. A. Marck, Axisymmetric rotating relativistic bodies: A new numerical approach for 'exact' solutions, Astron. Astrophys. **278**, 421 (1993).
[115] M. Ansorg, A. Kleinwachter, and R. Meinel, Highly accurate calculation of rotating neutron stars: Detailed description of the numerical methods, Astron. Astrophys. **405**, 711 (2003).
[116] N. Stergioulas, Rotating stars in relativity, Living Rev. Relativ. **6**, 3 (2003).
[117] S. Bonazzola, E. Gourgoulhon, and J.-A. Marck, Numerical approach for high precision 3-D relativistic star models, Phys. Rev. D **58**, 104020 (1998).
[118] http://www.gravity.phys.uwm.edu/rns.
[119] G. Pappas and T. A. Apostolatos, Revising the Multipole Moments of Numerical Spacetimes and its Consequences, Phys. Rev. Lett. **108**, 231104 (2012).
[120] S. M. Morsink, D. A. Leahy, C. Cadeau, and J. Braga, The oblate Schwarzschild approximation for light curves of rapidly rotating neutron stars, Astrophys. J. **663**, 1244 (2007).